Electronically Tunable Filters

by

Kevin Chang Yang

A thesis
presented to the University of Waterloo
in fulfillment of the
thesis requirement for the degree of
Master of Applied Science
in
Electrical and Computer Engineering

Waterloo, Ontario, Canada, 2016

AUTHOR'S DECLARATION

I hereby declare that I am the sole author of this thesis. This is a true copy of the thesis, including any required final revisions, as accepted by my examiners.

I understand that my thesis may be made electronically available to the public.

Kevin Chang Yang

Abstract

Microwave filters are essential building blocks in communications systems. As the communications industry evolves, smaller and more flexible filters with a high quality factor (high-Q) are in great demand. The deployment of tunability and reconfigurability in the designing of microwave filters provides greater system flexibility as well as economic benefits.

This thesis investigates a concept for improving the roll-off performance of filters that employ low-Q resonators. The approach is to combine two filters (sub-filters) with non-ideal characteristics to realize a band-pass filter with better roll-off characteristics, i.e. an effective high-Q value. Lossy filter and pre-optimization techniques are proposed to design the sub-filters.

To demonstrate the concept, two tunable band-pass filters are designed in microstrip, with slots etched on the ground plane as sub-filters. The sub-filters are simulated in the EM software, Sonnet. The simulated structures are fabricated, integrated with varactors, assembled, and then tested. The measured results are in good agreement with simulations, confirming the validity of the proposed concept. The thesis also investigates the use of the proposed concept in the design of tunable diplexers.

Acknowledgements

In 2010, after earning a degree in Actuarial Science, I started my first job as a data analyst in a bank. However, my passion for electrical engineering was constantly challenging my patience in the financial industry, while at the same time enhancing my desire to pursue a new career. Finally, after only one year at the bank, I decided to quit and start my Master program in electrical engineering. I began by learning Electromagnetics and RF engineering in undergrad classes.

In 2012, I enrolled in Dr. Raafat Mansour's graduate course, and then joined the CIRFE team in 2013. This marked the beginning of my exciting Master journey. As a student with limited background knowledge in electrical engineering, I was fortunate to be able to work with Dr. Mansour, who very generously offered his time, knowledge and expertise, and guided me through the enormous challenges of becoming an RF engineer. The processes of designing, simulating, fabricating and measuring would not have been accomplished without Dr. Mansour's careful instruction. I greatly appreciate the time and effort he devoted to my research.

I also wish to thank the external company who funded my research project. Mr. Bill Jolley, the lab manager at CIRFE, helped in assembling my circuits and trained me in numerous assembling techniques. I was deeply impressed by his expertise and patience during my work in the lab.

As well, I wish to express my sincere gratitude to my close friends and office mates, Dr. Scott Chen and Oliver Wong, who have always been ready to share their knowledge and support with me. My other colleagues, including Dr. Sara Attar, Ahmed Abdel Aziz, Mostafa Azizi, Frank Jiang and Jonny Jia, likewise experienced all the challenges and joys of Master studies together with me, and made my three-year experience rich and meaningful.

I could not have finished my research without the company of all my friends at Waterloo who are now studying or working at various places. To name a few: Zhenzhong Si, Miao Jiang, Wei Song, and Pete Zhao.

Finally, I wish to acknowledge my dear parents, Dr. Qian Wang and Mingdong Yang, who strongly supported me throughout my graduate studies. I have always been thankful for their wisdom and guidance, which have given me great confidence and perseverance in my life.

Dedication

To my beloved mother, Mingdong Yang, and father, Qian Wang,

and to Rongnan Wu, the best grandmother in the world.

Table of Contents

List of Figures

Chapter 1

Introduction

1.1 Motivations

High-quality factor (high-Q) tunable filters are needed in both wireless and satellite systems. The deployment of tunability and reconfigurability in these systems offers substantial flexibility and economic benefits. For example, one of the economic factors that wireless service providers value the most is the real-estate cost during base station installation in compact urban areas. Therefore, tunable filters that pack multiple functions (e.g., multistandards and multiband) into one site offer a large economic incentive for wireless service providers to incorporate them into the base station compared to traditional fixed-frequency filters. Furthermore, by employing tunable filters in satellite systems, one can significantly reduce the size and mass of the payload, due to multimode and multifunctional operation enabled by reconfigurability. This reduction in mass and size has a significant economic impact on the satellite system, as launch costs are positively correlated to satellite weight.

An ideal tunable filter must exhibit a high loaded-Q value. The loaded-Q value of the tunable filter is determined by the Q value of the filter structure itself and by the inherent loss of the tuning element in use. Various tuning elements are commonly employed in current systems, such as semiconductors [1]-[3], ferroelectric materials [4]-[5], ferromagnetic [6]-[8], and mechanical systems [9]-[12]. Integration of tuning elements with a filter degrades insertion loss performance, resulting in a lower loaded-Q value. Moreover, it is a major challenge to have a tunable filter with a high loaded-Q value over a wide tuning range.

1.2 Objectives

The principle objective of the present design is the provision of novel configurations for tunable band-pass filters that have an effective high loaded-Q value using low loaded-Q value resonators.

To achieve this goal, we propose using two sub-filters with relatively low-loaded Q values to realize a filter with an effective high loaded-Q value by making use of the following concepts:

1)   Wideband filters have low insertion loss, even if the resonators have low loaded Q-values.

2)   Better performance can be achieved from a filter at a band edge by optimizing the filter coupling matrix.

1

3)   Lossy filters, which inherently have low unloaded-Q, offer a sharp rejection out-of-band that is equivalent to the use of high-Q filters.

1.3 Thesis Outline

Following this introduction, Chapter 2 provides a review of major techniques of filter tuning, along with their advantages and disadvantages. These techniques include ferromagnetic material tuning, ferroelectric thin film tuning, RF MEMS tuning, and varactor tuning. Chapter 3 presents the concept, design, simulation and experimental results of a novel electronically tunable filter, highlighting the key advantages of this filter compared to other tunable filters. In addition, several conceptual frameworks of performance improvements on the structure built in Chapter 3 are illustrated. Finally, Chapter 5 summarizes the concepts, approaches and innovations of this research, and proposes potential improvements of the design as well as future research topics.

Chapter 2

Literature Survey

The four tuning methods reviewed in this section are: ferromagnetic material tuning, ferroelectric thin film tuning, RF MEMS tuning, and varactor tuning.

2.1 Ferromagnetic Material Tuning

Yttrium-Iron-Garnet (YIG) is the mostly commonly used tuning element in magnetic tunable filters. The resonator normally contains either a sphere crystal YIG or YIG films, which is a ferromagnetic material with chemical composition $Y_3Fe_2(FeO_4)_3$, or $Y_3Fe_5O_{12}$. Various tunable microwave band-pass and band-stop YIG filters are reported in [13-17].

YIG filters have several advantages. They have a high-Q factor in the order of 10,000, which is very high. They also have low insertion loss and excellent linearity. However, they tend to suffer from large power consumption (0.1-3.5 W) [18-19] as well as bulky size, heavy weight, and low tuning speed.

Krukpa et al. have reported two two-pole filters containing axial and circumferential magnetization of a ferrite material in [19] operating at around 2.2 GHz. The schematic diagrams of the proposed structure are shown in Figure 2.1. Pictures of both fabricated filters with axially magnetized ferrite rods and circumferentially magnetized ferrite disks are shown in Figure 2.2. From the measurement results in Figure 2.3, we can see these filters have very low insertion loss (< 0.8dB) and very good linearity.

| (a) | (b) |
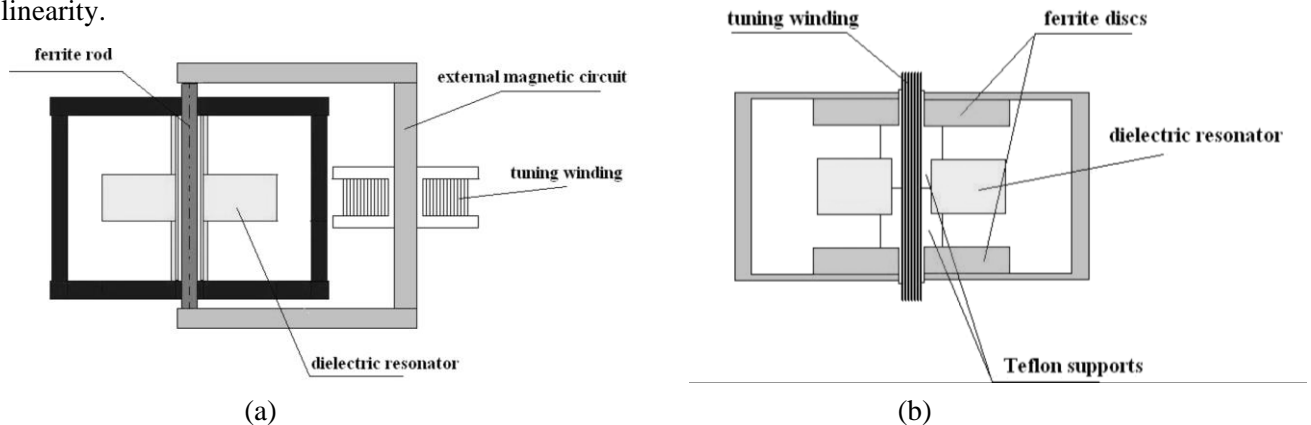
Figure 2.1 Schematic diagram of tunable dielectric resonators containing (a) axially and (b) circumferentially magnetized ferrite elements [19]

3
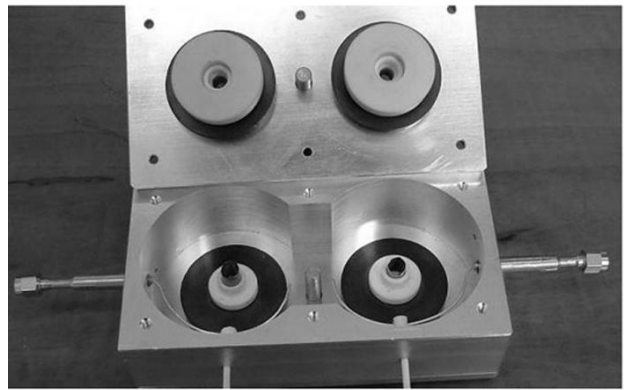
(a)   (b)

Figure 2.2 Pictures of tunable filters: (a) a filter containing axially magnetized ferrite rods, and (b) a disassembled filter containing circumferentially magnetized ferrite disks [19]
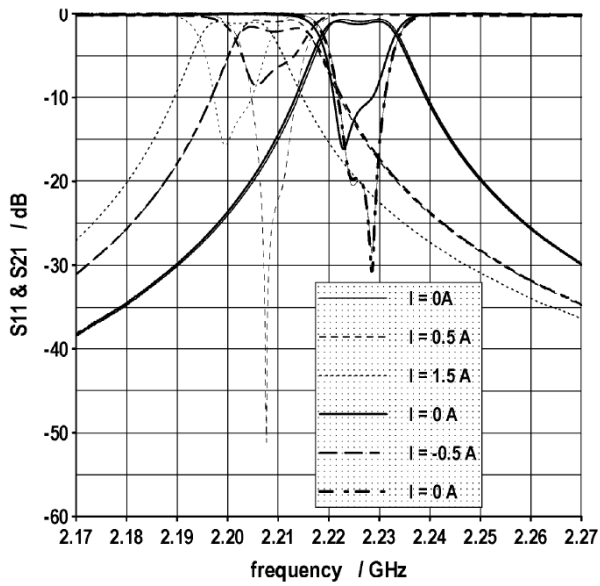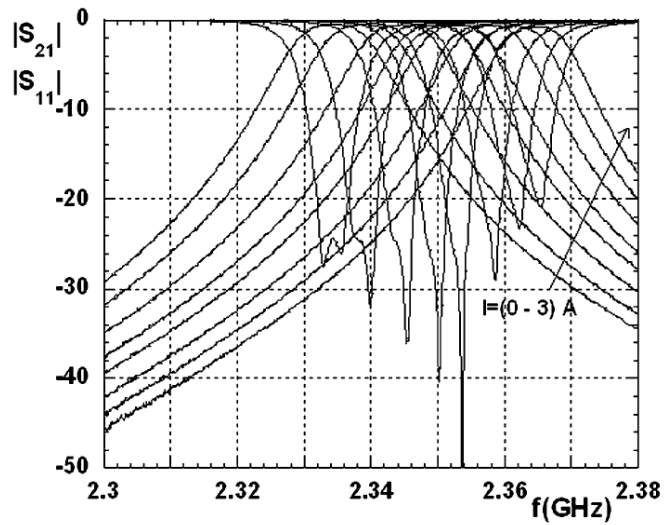
(a)   (b)

Figure 2.3 (a) Measured characteristics for the filter containing axially magnetized ferrite rods, and (b) measured characteristics for the filter containing circumferentially magnetized ferrite discs [19]

4

2.2 Ferroelectric Thin Film Tuning

A Barium Strontium Titanate (BST) tunable filter uses ferroelectric thin film material with the chemical composition of $(Ba_xSr_{1-x})TiO_3$ as a tuning element [20]. The dielectric constant of this type of ferroelectric thin film can be changed when a DC bias voltage is applied to the ferroelectric film. Therefore, this property is widely used in fabricating tunable capacitors or varactors.

Various BST varactors have been reported in [22-28] for tunable filters. Compared with other tuning elements, the major advantages of BST varactors are that they are small in size, are planar (which means they are easy to integrate), and have a wide tuning range and a fast tuning speed. They also have superb power-handling capability.

Figure 2.4 shows a block diagram of a dual-mode filter and a cross-sectional view of a test device with a multilayer (BST/TiO2/Si) structure [21]. Figure 2.5 shows the capacitance dependence and resonance frequency of the BST thin films grown on a TiO2/Si and MgO substrate against applied voltage from 0 to 40 V [21]. Figure 2.6 shows the insertion loss and return loss with DC bias voltages of 0 V, 20 V, and 40 V for the BST dual-mode filter fabricated on TiO2/Si and MgO substrates, respectively.
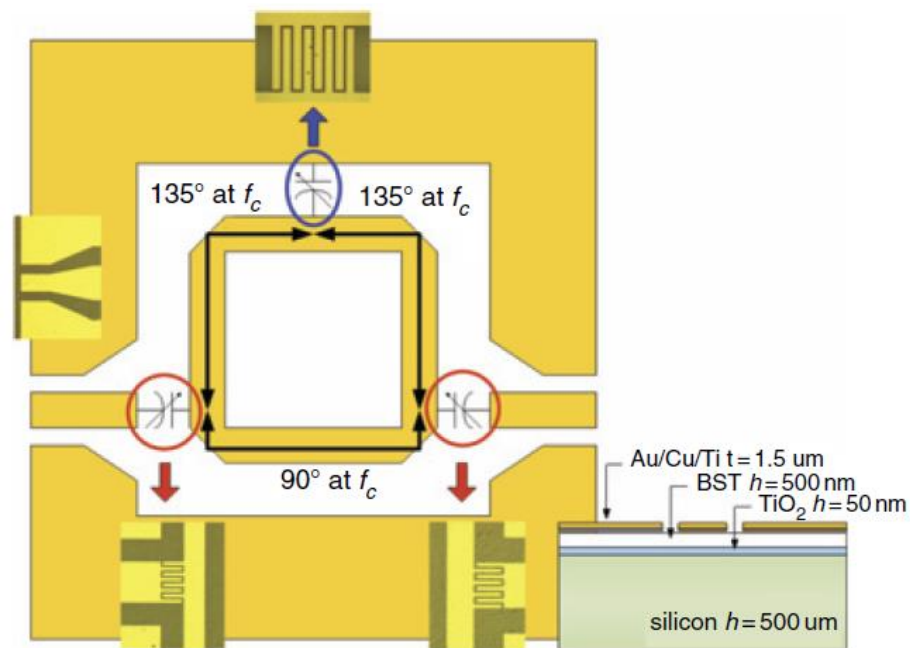
Figure 2.4 Block diagram for dual-mode filter and cross-sectional view of test device with multilayer (BST/TiO2/Si) structure [21]
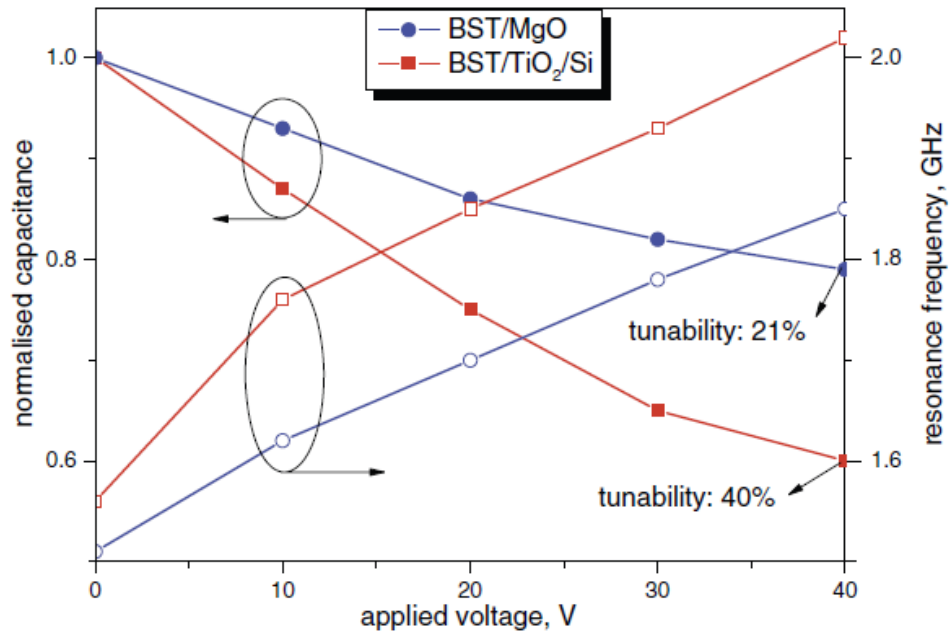
Figure 2.5 Normalised capacitance and resonance frequency against frequency with applied voltages for BST dual-mode filter fabricated on TiO₂/Si and MgO substrate [21]

—■— **normalised capacitance on TiO2/Si substrate due to applied voltages**

—●— **normalised capacitance on MgO substrate due to applied voltages**

—□— **resonance frequency on TiO2/Si substrate due to applied voltages**

—○— **resonance frequency on MgO substrate due to applied voltages**
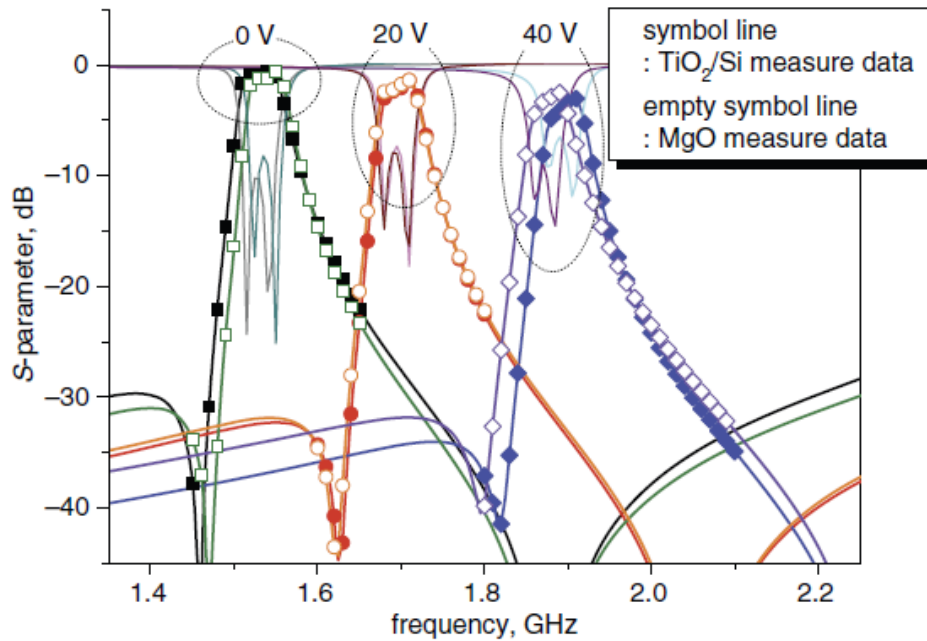
Figure 2.6 Measured results of frequency responses for dual-mode filter [21]

2.3 RF MEMS Tuning

The radio frequency microelectromechanical system (RF MEMS) is a type of electro-mechanical device that is fabricated using micro-machining technology. It usually contains a capacitor network for changing capacitance value by applying DC voltage or a capacitive switch for "on" and "off" switching. The main advantages of RF MEMS is its low loss and low distortion levels [29-30]. It is also very small in size, which makes it easy to integrate. However, RF MEMS tuning elements are very fragile and require very careful packaging, and they also suffer from reliability issues.

Fourn et al. presented a tuning interdigital planar filter employing MEMS capacitors [31]. Figure 2.7 shows the structure of the "on" and "off" state of the MEMS capacitive cantilever switch, while Figure 2.8 shows their fabricated filter with the MEMS switch integrated around the center of the structure. In their article, the researchers reported a two-pole tunable filter with a 13% relative bandwidth with switchable center frequency from 18.5 to 21.05 GHz. The return loss of this planar filter is less than 15 dB and the insertion loss is 3.5 dB. Figure 2.9 shows Fourn et al.'s simulated and measured responses of the tunable filter.

7
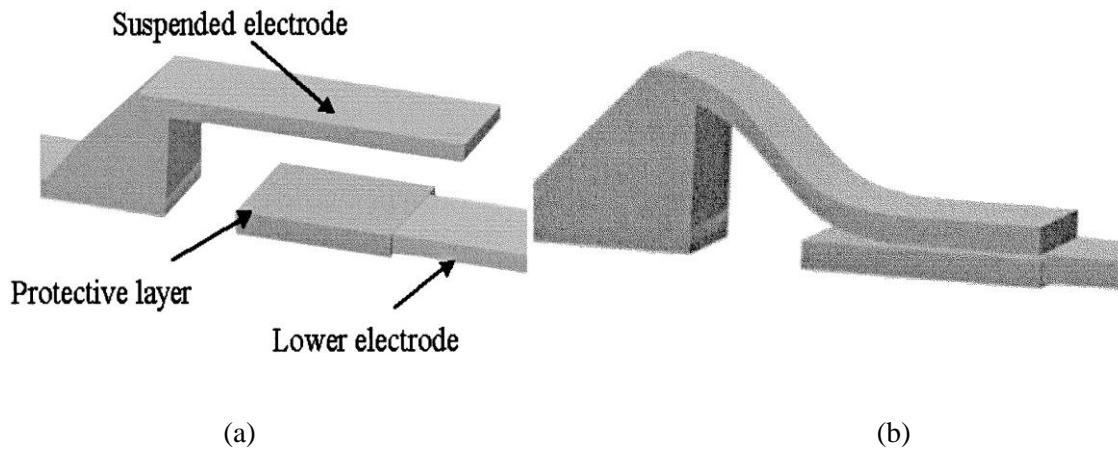
Figure 2.7 Drawing of a MEMS capacitive cantilever switch: (a) in the "off" state, and (b) in the "on" state [31]
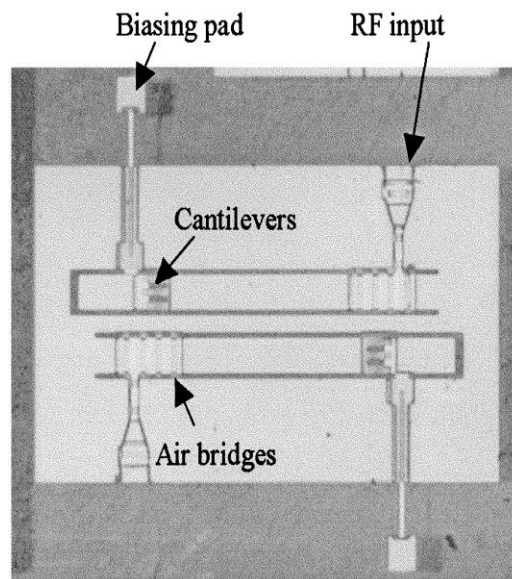
Figure 2.8 Microphotograph of the fabricated filter [31]
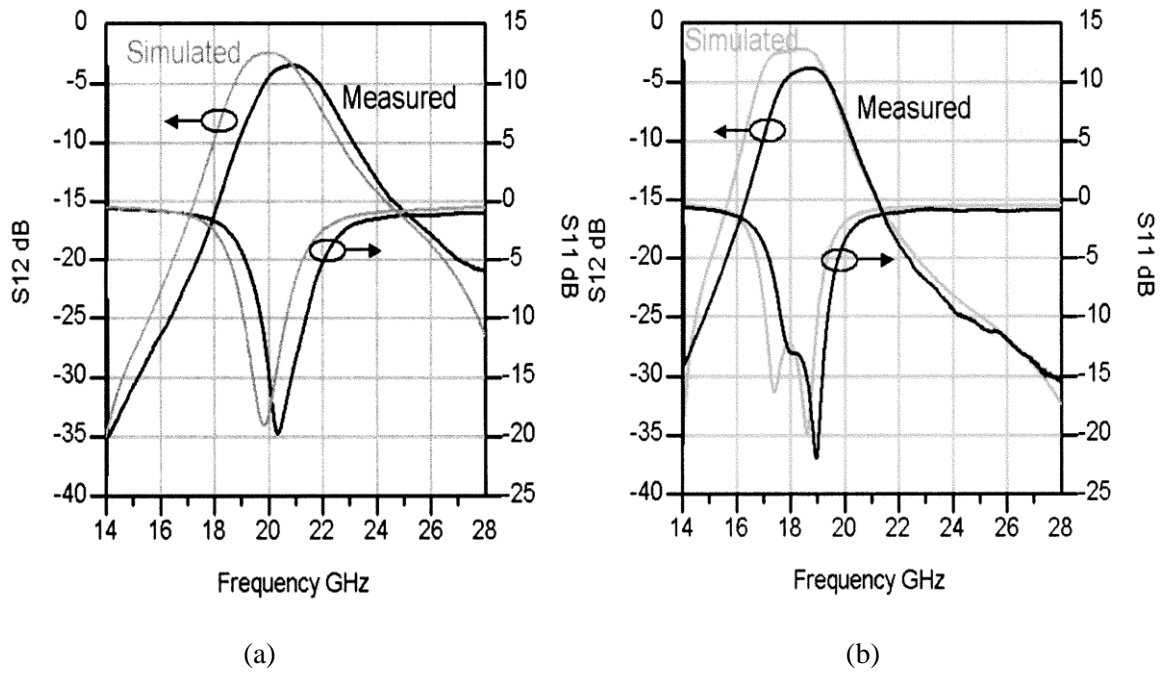
Figure 2.9 Simulated and measured responses of the tunable filter: (a) switches up, and (b) switches down [31]

2.4 Semiconductor Varactor Tuning

A semiconductor variable capacitance diode, or a varactor diode, is a special PN junction diode that is operated with reverse-bias DC voltage. When a varactor diode is reverse-biased, there is no current flow which is equivalent to infinite resistance. Hence, the diode is effectively acting as a capacitance. The tunability of the capacitance comes from the change in the width of the depletion region when the applied reverse-bias DC voltage varies [32].

Filters employing semiconductor varactors have zero power consumption. They also have a very high tuning speed and are extremely small in size, making them more attractive compared to the conventional YIG and BTS filters for modern communication systems [33]. However, moderate Q and non-linearity are some of the drawbacks of this tuning method.

In [2], Brown et al. reported a capacitively-loaded interdigital tunable filter with a suspended substrate stripline and varactor diodes. The diodes are connected at the end of each interdigital finger, as shown in Figure 2.10. The picture of the fabricated filter is shown in Figure 2.11. The fabricated

9

filter is measured to have a 60% tuning bandwidth from 700MHz to 1.33 GHz and a relatively low insertion loss, as illustrated in Figure 2.12. Since the filter suffers from bandwidth degradation while tuning, the researchers also investigated the relationship between center frequency and relative bandwidth as a function of bias voltage.
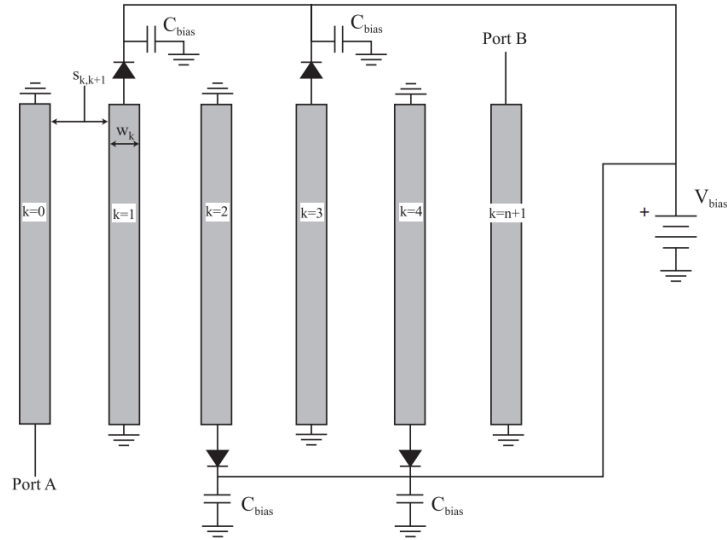
Figure 2.10 Topology of the varactor-loaded interdigital band-pass filter [34]
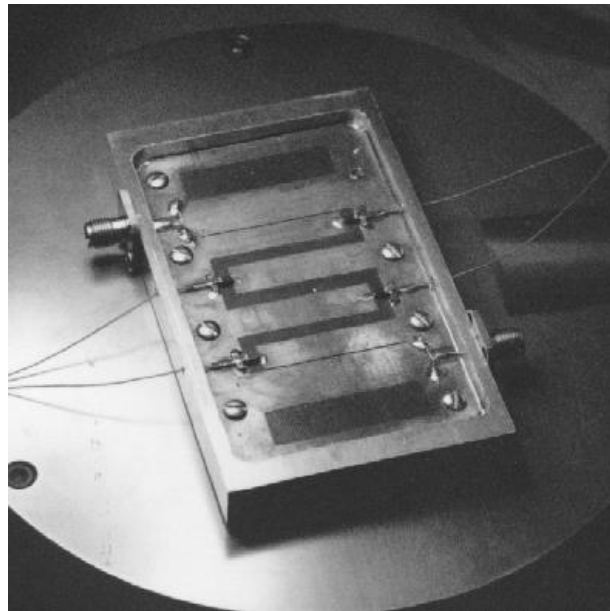
Figure 2.11 The RF varactor-tuned band-pass filter [34]
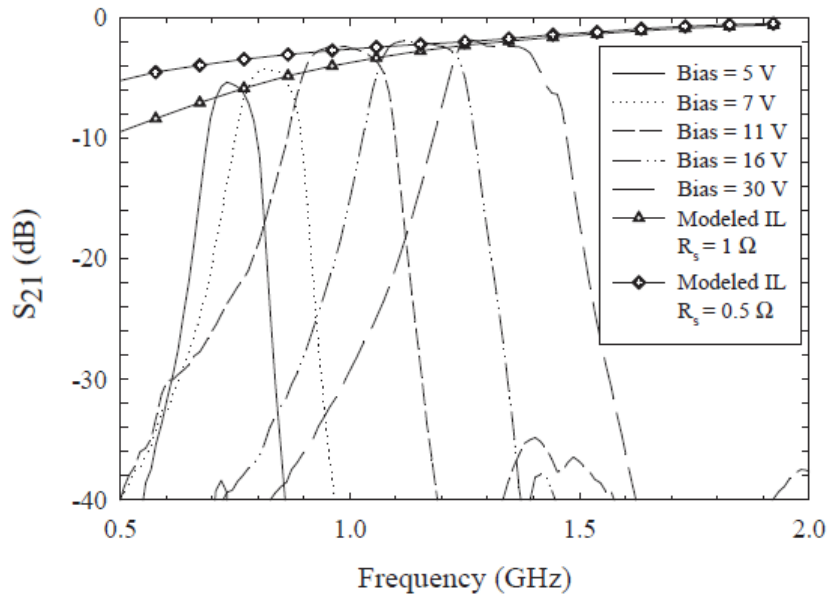
(a)
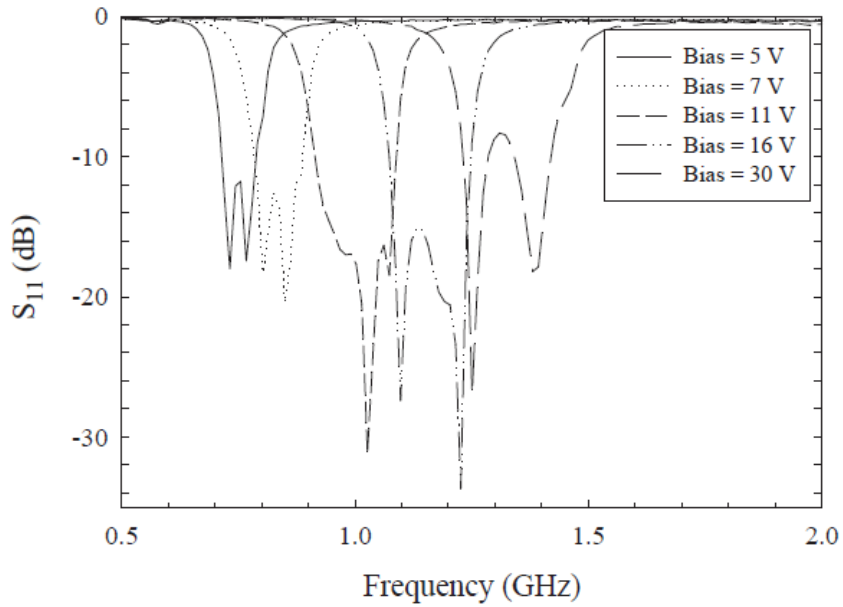
(b)

Figure 2.12 RF tunable filter: (a) measured insertion loss, and (b) return loss for various bias levels [34]

Chapter 3

Tunable Band-pass Filter Employing Two Band-Stop Filters

3.1 Introduction

In the communications systems, it is highly desirable to have a tunable filter with a high loaded-Q value. However, the loaded-Q value of the tunable filter is determined by the Q value of the filter structure itself, as well as by the inherent loss of the tuning element in use. Integrating tuning elements with the filter degrades insertion loss performance and results in a lower loaded-Q value.

In the majority of papers published on tunable filters, a constant bandwidth could not be maintained over the tuning range because only the resonators are tuned, while the inter-resonator couplings are left untouched.

Our proposed filter also applies tuning elements only to resonators, but with a different approach. It employs two band-stop sub-filters to realize a tunable band-pass filter that is tunable both in center frequency and bandwidth. The concept yields an enhanced filter performance, making use of the following:

a) S21 of the band-stop sub-filter in the passband (Figure 3.1 (a), Region A) is less dependent on the Q of tuning elements and is also less dependent on the variation of the inter-resonator coupling.

b) The sharpness of S11 of the band-stop sub-filter in the stop-band (Figure 3.1 (b) Region B) can be improved by scarifying the performance of the passband.

The concept here is to use two tunable band-stop sub-filters – S21 in region A from the first sub-filter and S11 in region B from the second sub-filter – to deliver a band-pass filter with tunability in both the centre frequency and bandwidth that is least dependent on the resonator Q and variation of the inter-resonator coupling over the tuning range.
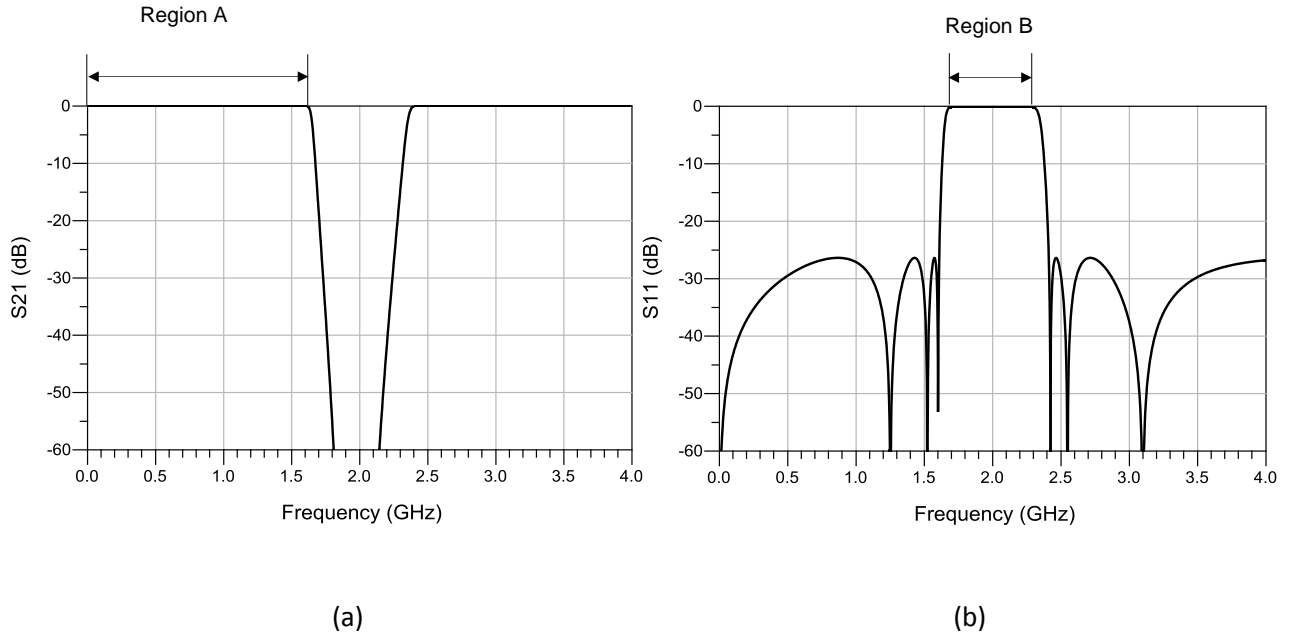
Figure 3.1 Regions of interest in S_{21} and S_{11} of a band-stop sub-filter

3.2 Proposed Concept

Figure 3.2 shows the proposed concept for constructing a band-pass filter. As demonstrated in Figure 3.2 (a), as the input signal propagates through the first band-stop sub-filter, F1, the signal in region A (DC to f1 in Figure 3.2 (b)) enters circulator C1. This, in turn, directs the incoming signal into the second band-stop sub-filter, F2, which is terminated with a 50 Ω matched load. All signals that pass through F2 get absorbed by the matched load, except those in region B (f2 to f2' in Figure 3.2 (b)), where the signals get reflected by the stop-band of F2. The combination of F1, F2 and C1 guarantees that signals covering the band of interest reach F2, and that F2 only reflects signals in the frequency range between f1 and f2 back into C1. Consequently, a pass-band of f1 to f2 is synthesized and directed by C1 to the output port.
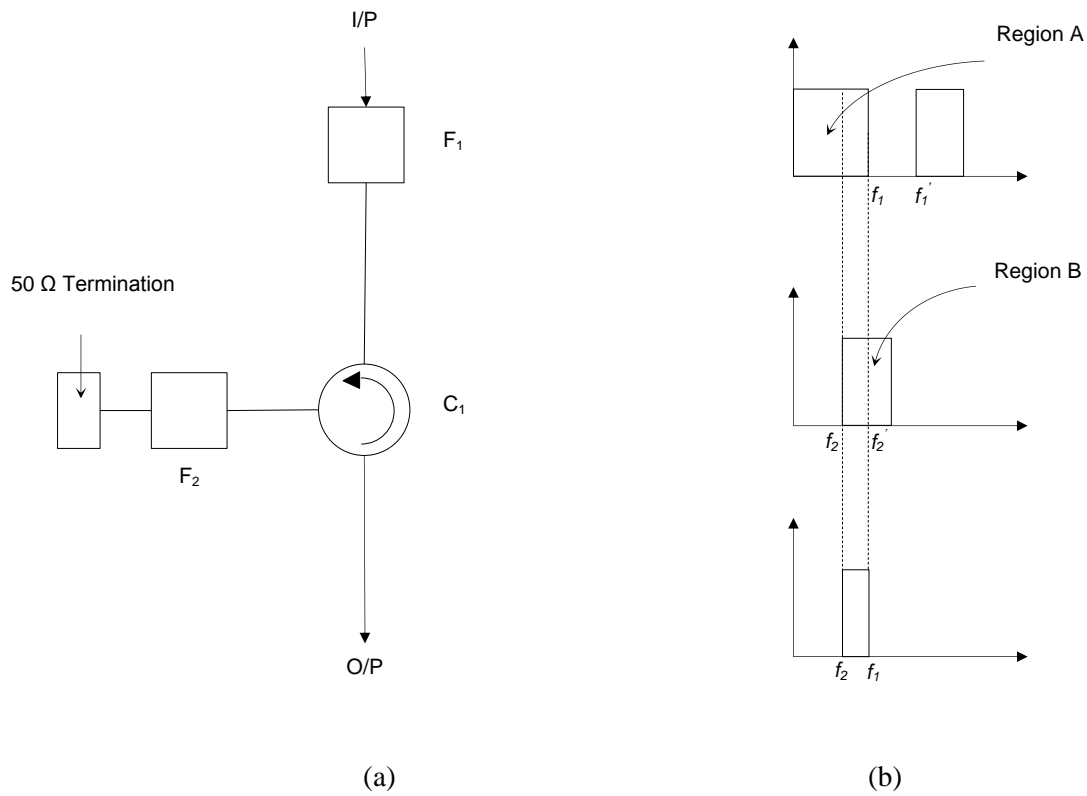
Figure 3.2 Concept chart of band-pass filter structure based on two band-stop sub-filters and one circulator

3.3 Band-pass Filter Design

3.3.1 Base Sub-filter Model

While the concept can be applied to any tunable band-stop filter, we are going to demonstrate the concept using a band-stop filter similar to the one reported in [36] as a base model, as shown in Figure 3.3. This type of filter offers a very good insertion loss in region A of Figure 3.1, since the insertion loss is mainly determined by the loss of the microstrip line. One example is taken from [36], as shown in Figure 3.4
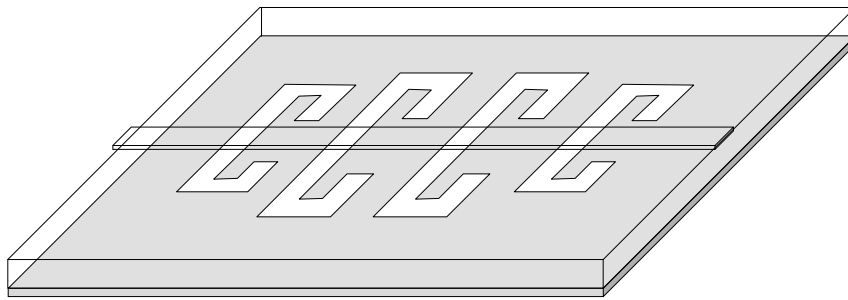
Figure 3.3 A four-pole microstrip filter employing non-uniform metal-loaded slots in the ground plane [36]

Region A
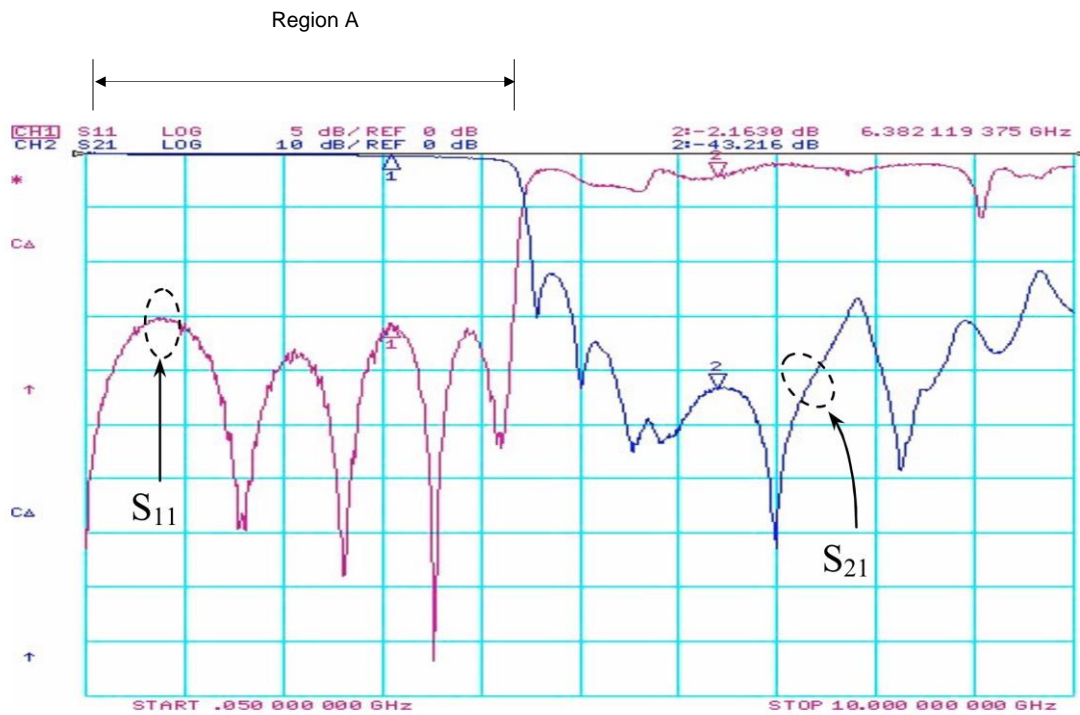
Figure 3.4 Measured result of an eight-pole microstrip filter presented in [36], employing non-uniform metal-loaded slots in the ground plane

15

3.3.2 Tunability Analysis

In order to develop a tunable filter, we first need to analyze the tunability of the tuning elements, including the tuning range, loss, and linearity. Sonnet software is used in this analysis for EM simulation, and ADS is used for reading measured results on tunabilities.

When varactors are placed at different positions on the filter structure, the tuning range of the filter varies. Therefore, various positions of the tuning elements are simulated in Sonnet. From these simulation results, the one with the widest tuning range is selected for later fabrication.

Figure 3.5 shows one of the possible placements of varactors on metal-loaded slots in our filter design.
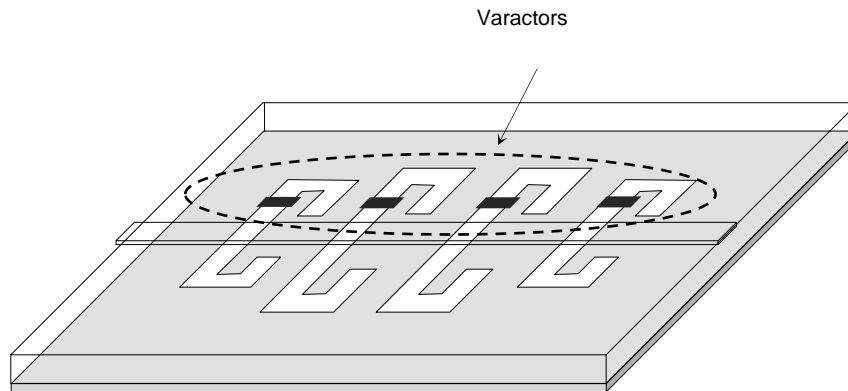
Varactors

Figure 3.5 A four-pole microstrip filter employing uniform metal-loaded slots in the ground plane, where varactors are loaded onto metal-loaded slots on the ground plane of a 50 Ω microstrip line

Multiple positions of varactors on the slots are simulated and analyzed. The tunability has a clear trend as the position of the varactors move from the far end of the metal slots towards the center. Figure 3.6 shows two of these position setups: one is at the far end of the metal slots, and the other is at a position near the center of the slots.
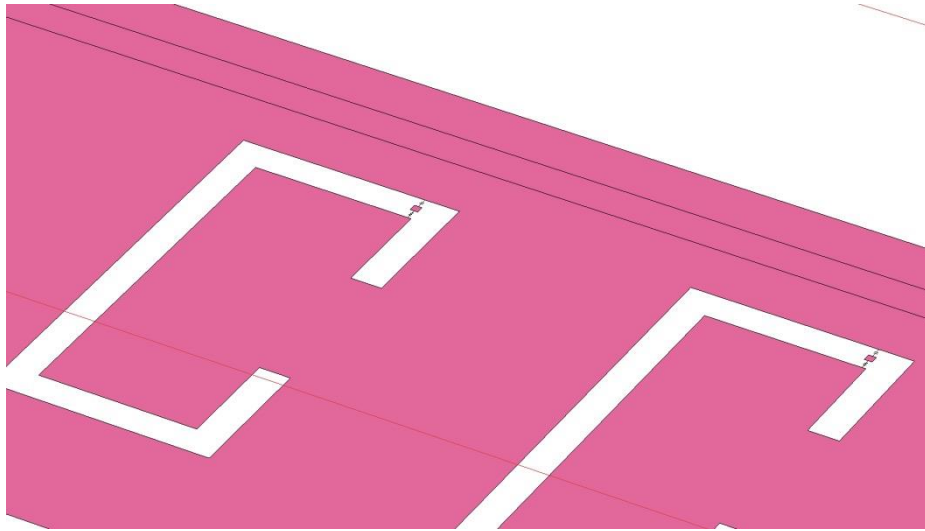
(a)
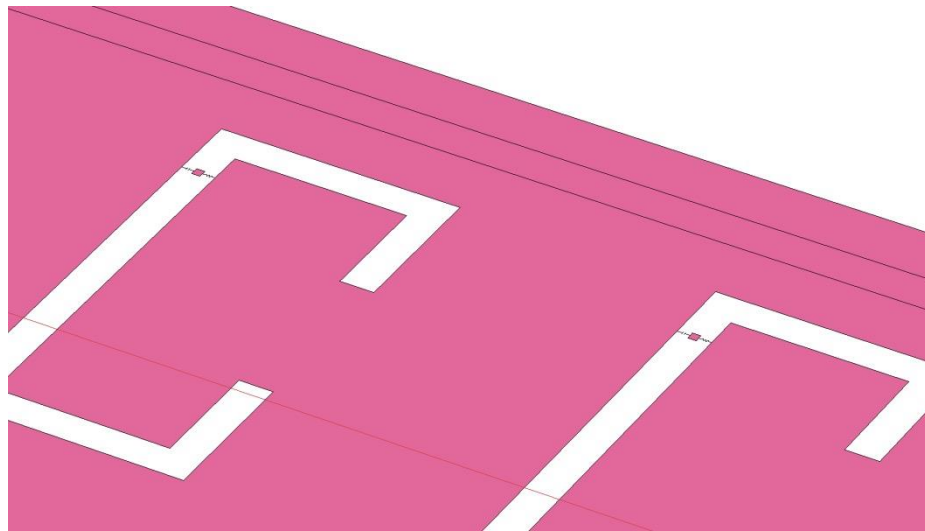
(b)

Figure 3.6 Two varactor-position setups on metal slots: (a) far end, and (b) close-to-center

Figure 3.7 shows the Sonnet simulation results of these two varactor-position setups. The blue line shows the tuning range of the filter when varactors are placed in the far-end position of the slots, while the pink line shows the tuning range of the filter when varactors are placed in the close-to-center position of the slots. It can be seen from Figure 3.7 that, when placed at a position close to the center, the filter has the highest tunability. Therefore, a position that is close to the center is chosen for assembling our varactors.
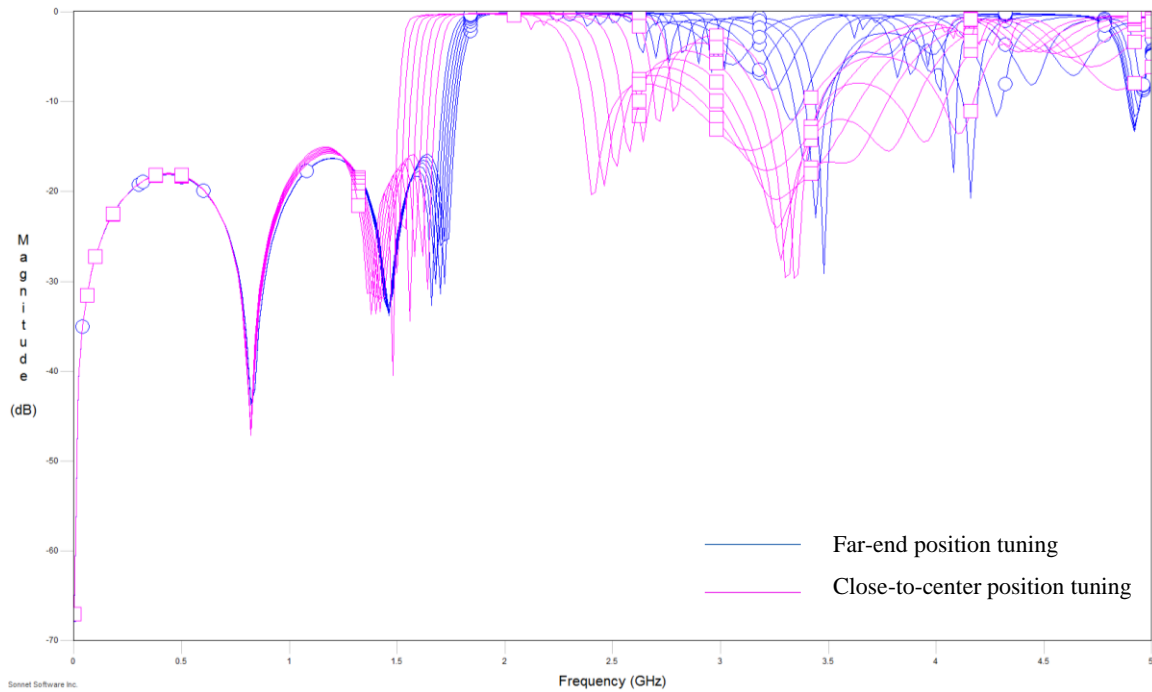
Figure 3.7 Comparison of tuning results of two varactor-position setups in Sonnet

3.3.3 Linearity Analysis

This section presents two types of varactors that were tested and measured at the CIRFE (Centre for Integrated RF Engineering) lab by Oliver Wong. One is MTV4030-02-11 from Cobham Metelics (formerly Aeroflex / Metelics), and the other is MA46603-134 from M/A-COM Technology Solutions Holdings, Inc.

   Figure 3.8 shows the graph of Capacitance vs. Applied DC Voltage between frequency 0 GHz and 9 GHz for varactor MTV4030-02-11.
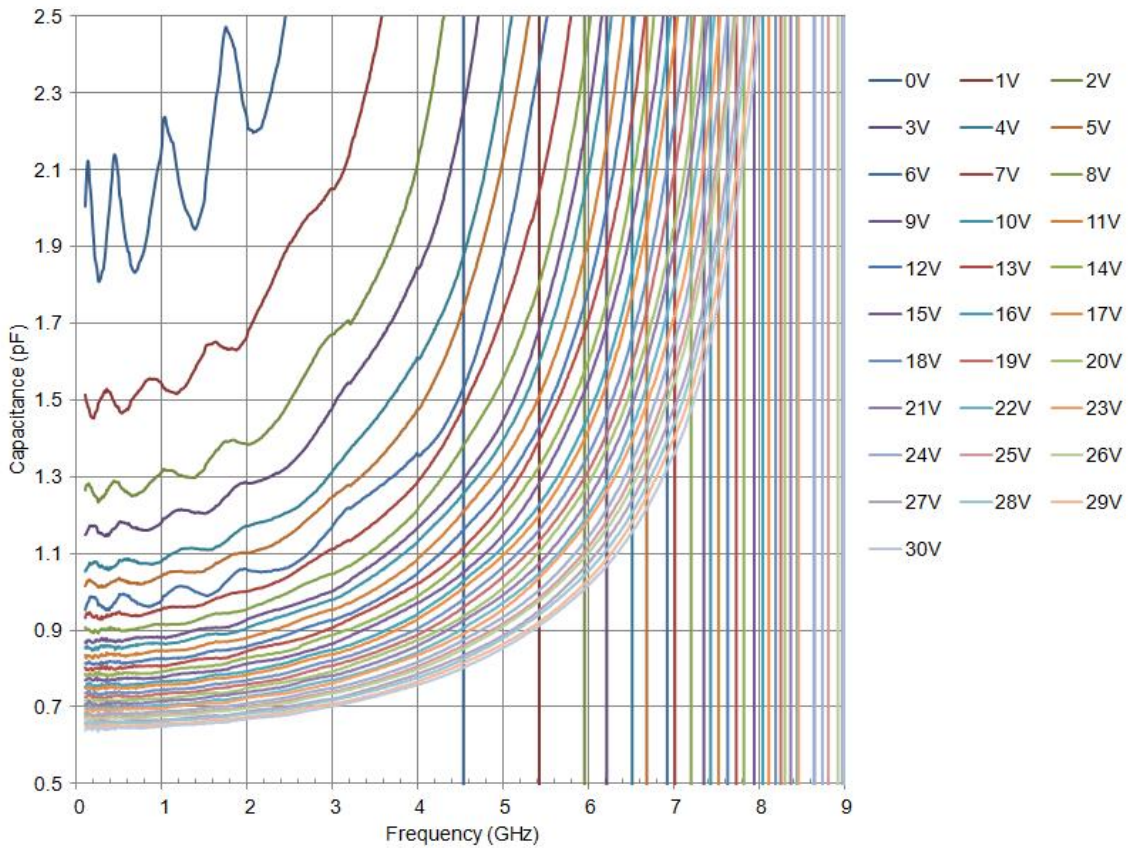
Figure 3.8 Measured Aeroflex varactor MTV4030-02-11 Capacitance vs. Applied DC Voltage curve, by Oliver Wong, CIRFE

Figure 3.9 shows the graph of Capacitance vs. Applied DC Voltage between frequency 0 GHz and 10 GHz for varactor MA46603-134.
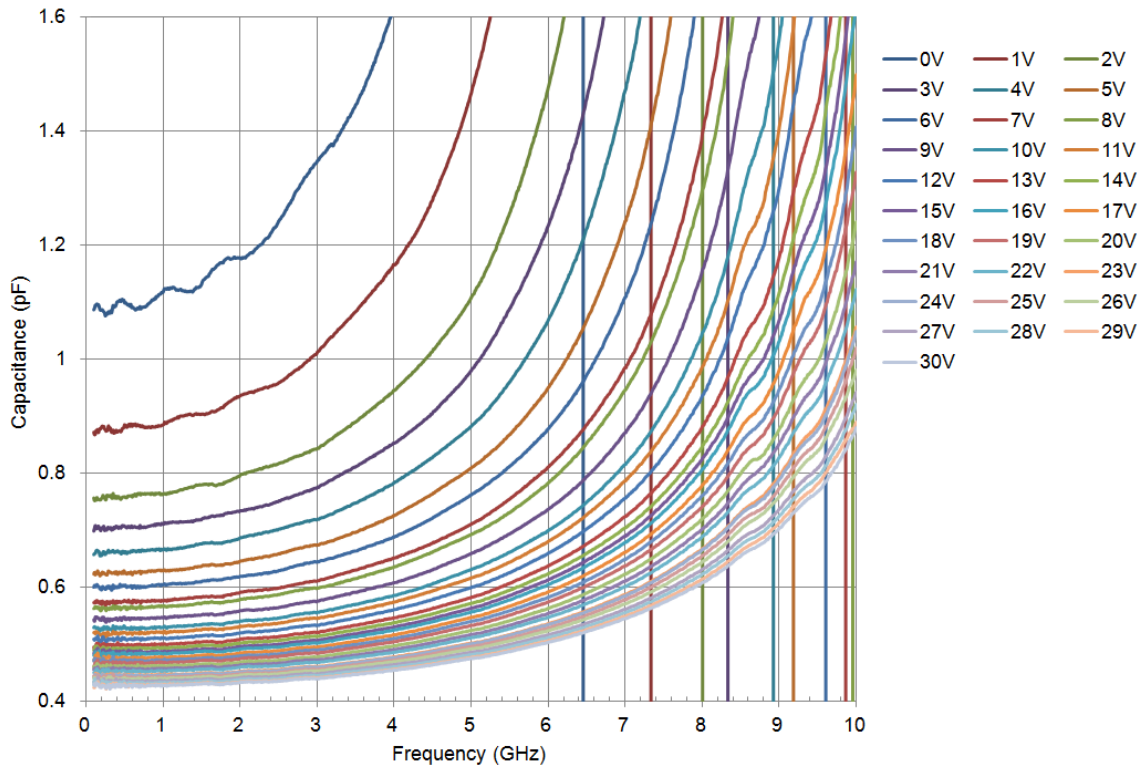
Figure 3.9 Measured MA/COM varactors MA46603-134 Capacitance vs. Applied DC Voltage curve, by Oliver Wong, CIRFE

Since our design target is to have a tunable filter with a center frequency of around 2 GHz, we are mainly interested in the area around 2 GHz in Figure 3.8 and Figure 3.9. The capacitance of both varactors has very decent linearity in the low voltage range (from 2 V to 10 V). However, when the applied voltage is low (0 V to 6 V), MTV4030-02-11 has a very large variance in capacitance around our frequency range of interest, compared to MA46603-134. Therefore, MA46603-134 is a better choice between these two types of varactors for our research purposes.

3.3.4 Simulation Results

Figure 3.10 shows the EM simulation results for the three tuning states of the band-stop sub-filter shown in Figure 3.5. Figure 3.11 shows the EM simulation results of a tunable band-pass filter using two of the sub-filter structures shown in Figure 3.5, employing the concept presented in Figure 3.2. This filter has a constant 3-dB bandwidth of 300 MHz at 2 GHz.
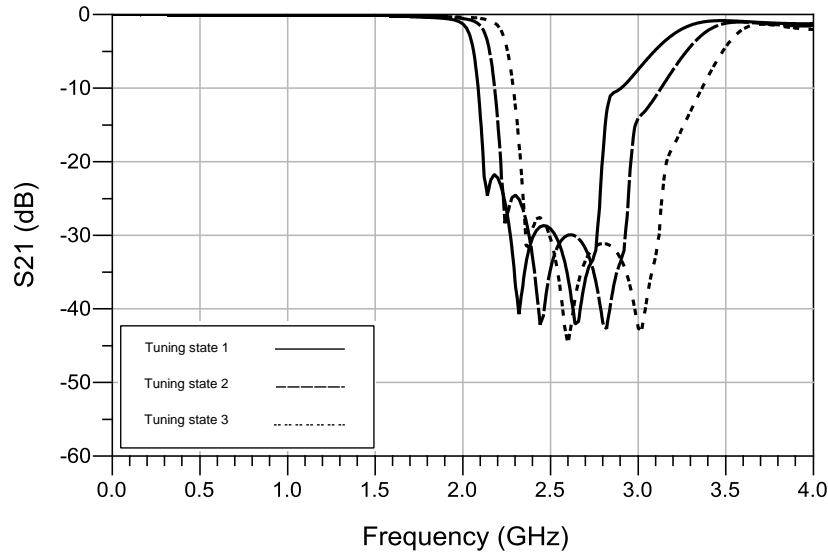
Figure 3.10 EM simulation of three tuning states for the proposed band-stop sub-filter
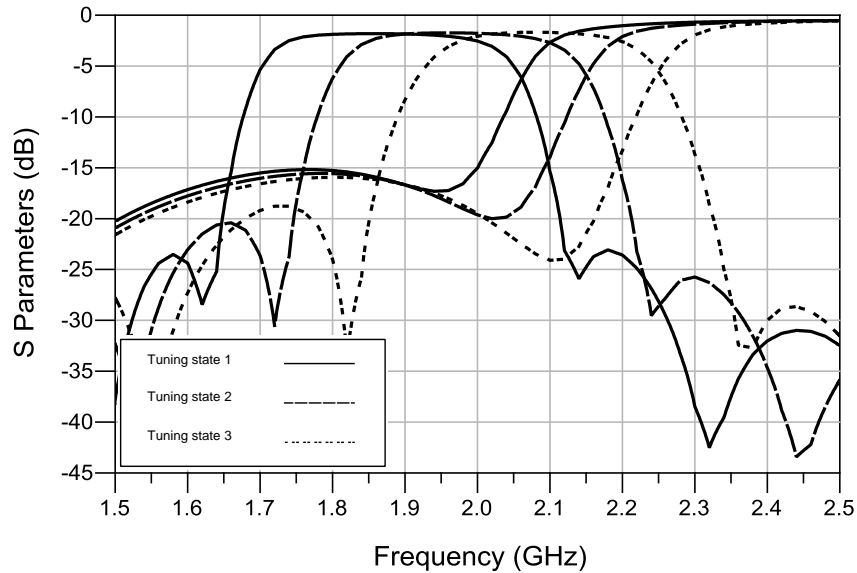
Figure 3.11 EM simulation results of the tunable band-pass filter

3.4 Measurement Results

Pictures of one of the fabricated band-stop sub-filters are presented in Figure 3.12. Figure 3.12 (a) also shows the additional pads etched on the ground plane for applying DC bias voltage onto the varactors.
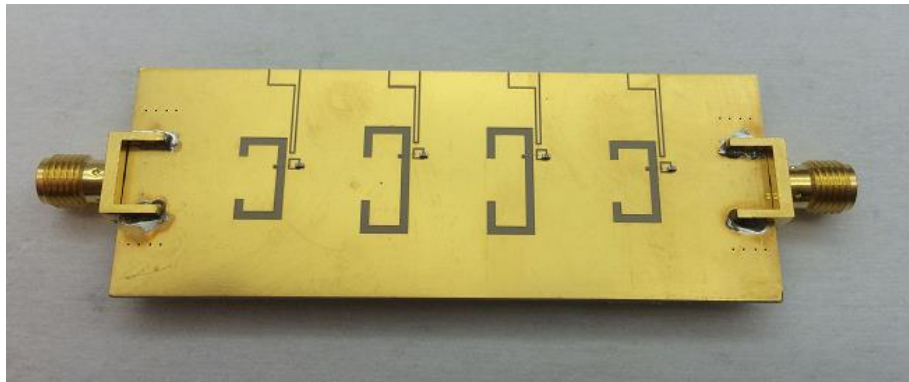
(a)
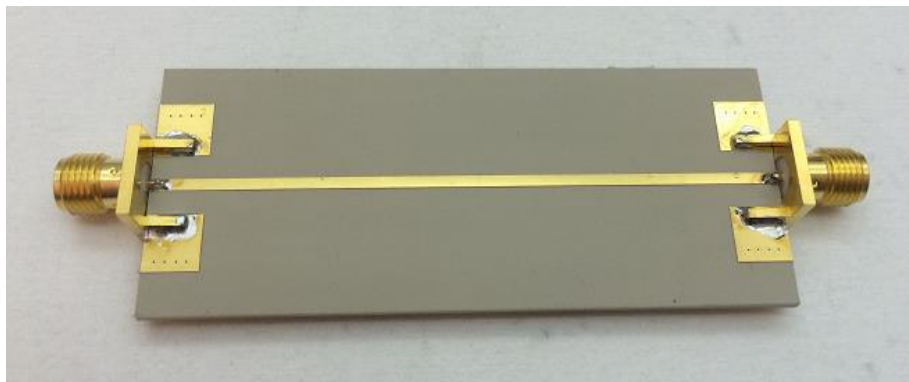
(b)

Figure 3.12 Fabricated band-stop sub-filters with non-uniform metal-loaded slots etched on the ground plane: (a) top view, and (b) bottom view

Figure 3.13 presents the measured results of the tunability of both regions A and B of the fabricated band-stop sub-filters, F1 and F2, respectively. The voltage applied to the varactors in Figure 3.13 (a) ranges from 0 V to 4 V. The voltage applied in Figure 3.13 (b) ranges from 0 V to 20 V. The applied

DC bias voltages are tuned continuously; however, Figure 3.13 (a) displays only three tuning states of the F1 that give the same amount of frequency shift as the three states for F2, as shown in Figure 3.13 (b).
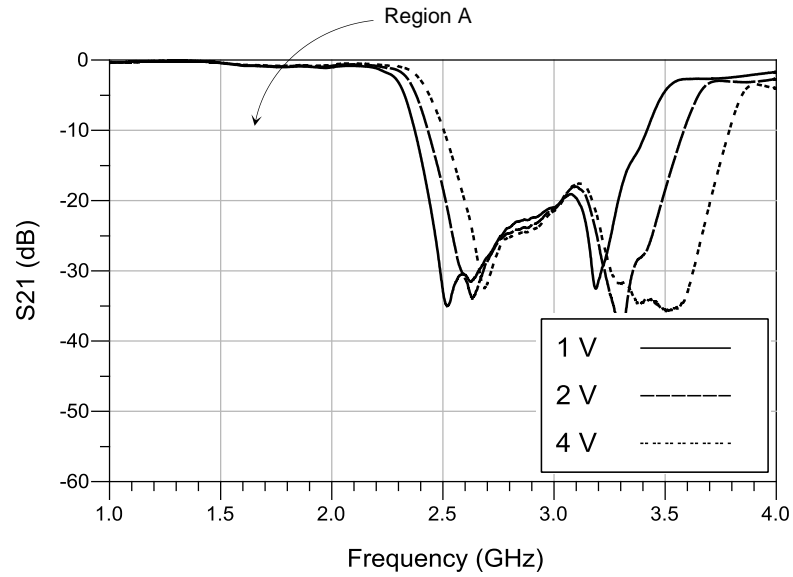
(a)
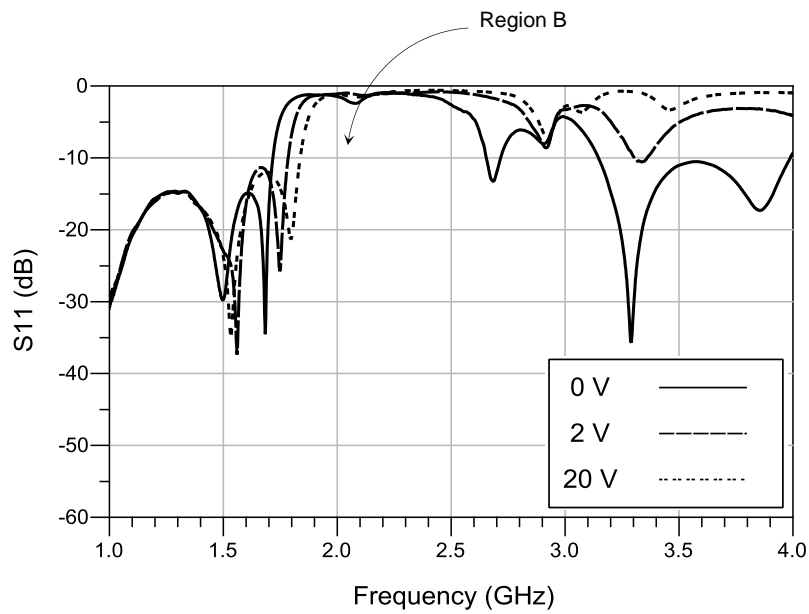
(b)

Figure 3.13 Illustrated chart showing: (a) three measured tuning states of region A in F_1, and (b) three measured tuning states of region B in F_2

A picture of a fabricated and assembled tunable band-pass filter consisting of two tunable band-stop sub-filters and one circulator is given in Figure 3.14.

The measured results of this structure are presented in Figure 3.15. It can be seen that the filter has a relatively constant 3-dB bandwidth of 300 MHz over the tuning range. The insertion loss ranges from 2.3 dB to 3.1 dB within the tunable passband without metallic housing. A portion of this insertion loss is attributed to the loss of the circulator and radiation, since the filters were not packaged in this prototype unit. With the use of packaging and a low loss circulator design, a much better insertion loss performance can be potentially achieved.

It should be noted that both the S_{11} and S_{21} exhibit high values in at the lower-frequency range (up to 1.7GHz) due to the fact that the RF energy in this frequency range is dissipated in the 50-ohm load. In addition, the ripple seen in the measurement results can be attributed to multiple reflection and mismatch among SMA-SMA connectors and the circulator. It should be also mentioned that the results shown in Figure 3.15 are obtained by applying the same DC bias voltage to all four varators. A much better performance can be achieved through non-synchronous tuning, where the DC bias voltages for the varators are tuned to optimize the overall filter performance.

Figure 3.14 Fabricated and assembled tunable band-pass filter
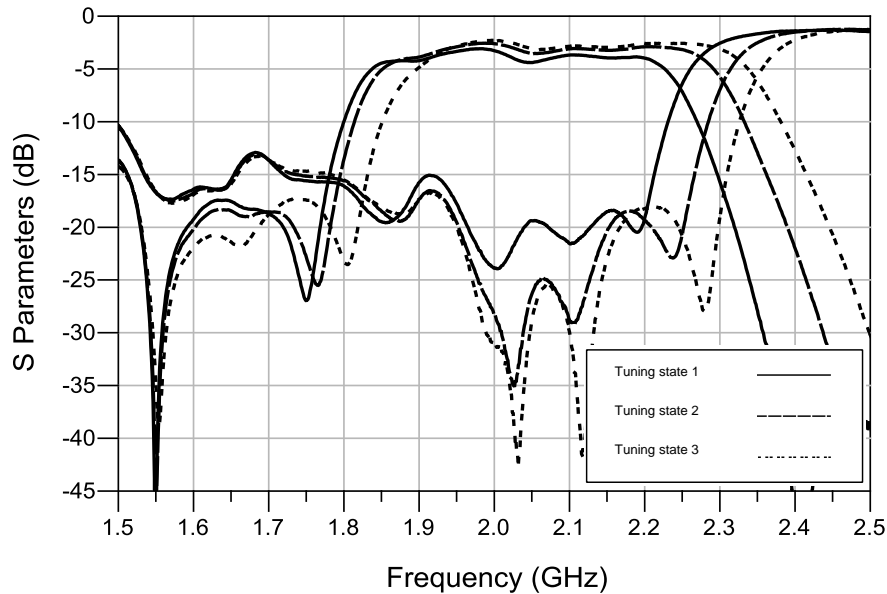
Figure 3.15 Measured results for the tunable band-pass filter

Figure 3.16 show a picture of another setup of a tunable band-pass filter. The difference between Figure 3.14 and Figure 3.16 is that the latter is constructed of two identical tunable band-stop sub-filters from the left-side of the former structure.

The reason for this setup is that the sub-filter on the left in Figure 3.14 has a much wider tuning range than that on the right. The measured tuning ranges of both filters are shown in Figure 3.17 and Figure 3.18, respectively. In order to improve the tuning range of the combined band-pass filter, the band-stop sub-filter with a wider tuning range is used for both sides of the band-pass filter structure. Furthermore, when in operation, the sub-filter on the left side of Figure 3.16 needs to operate at a higher frequency by tuning the varactors in order to realize a band-pass filter structure.
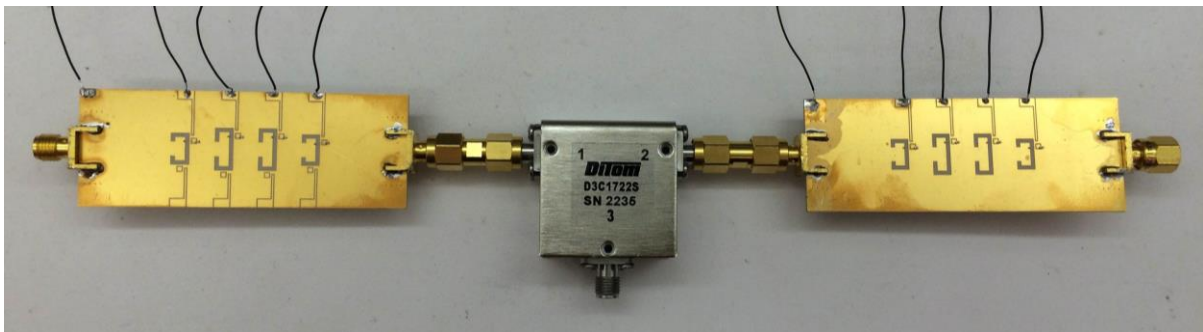
Figure 3.16 Fabricated and assembled tunable band-pass filter with two identical sub-filters

25
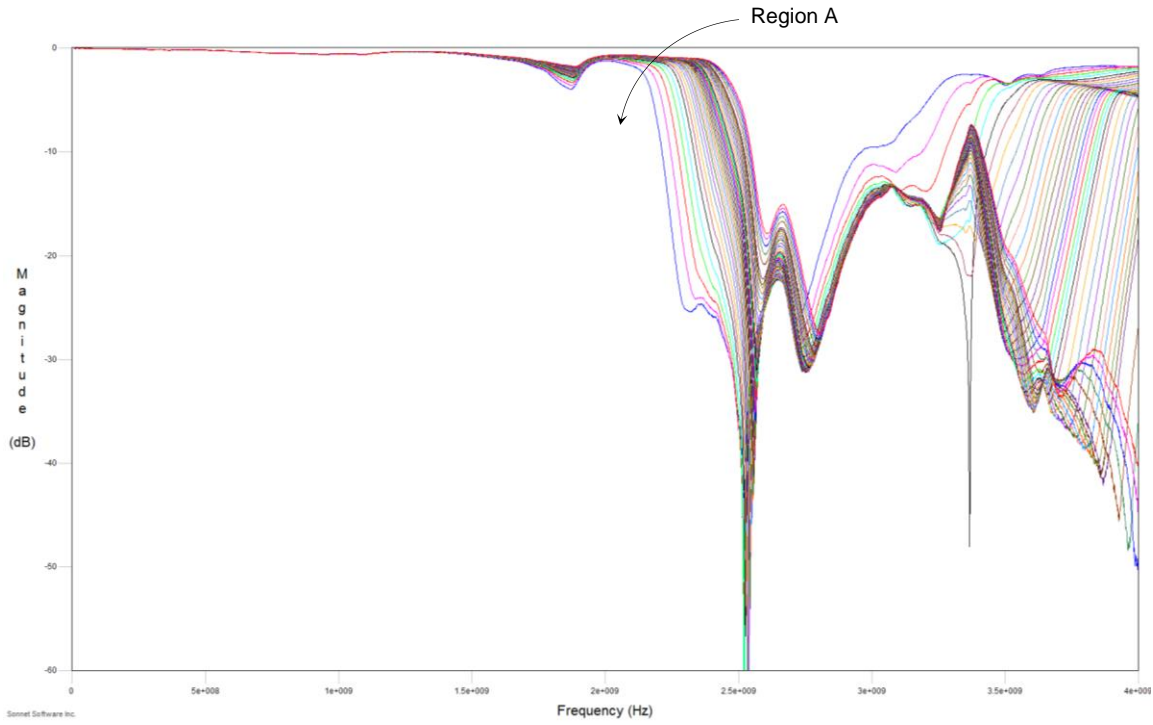
Figure 3.17 Measured tuning range of the left sub-filter in Figure 3.14 from 0 V to 20 V
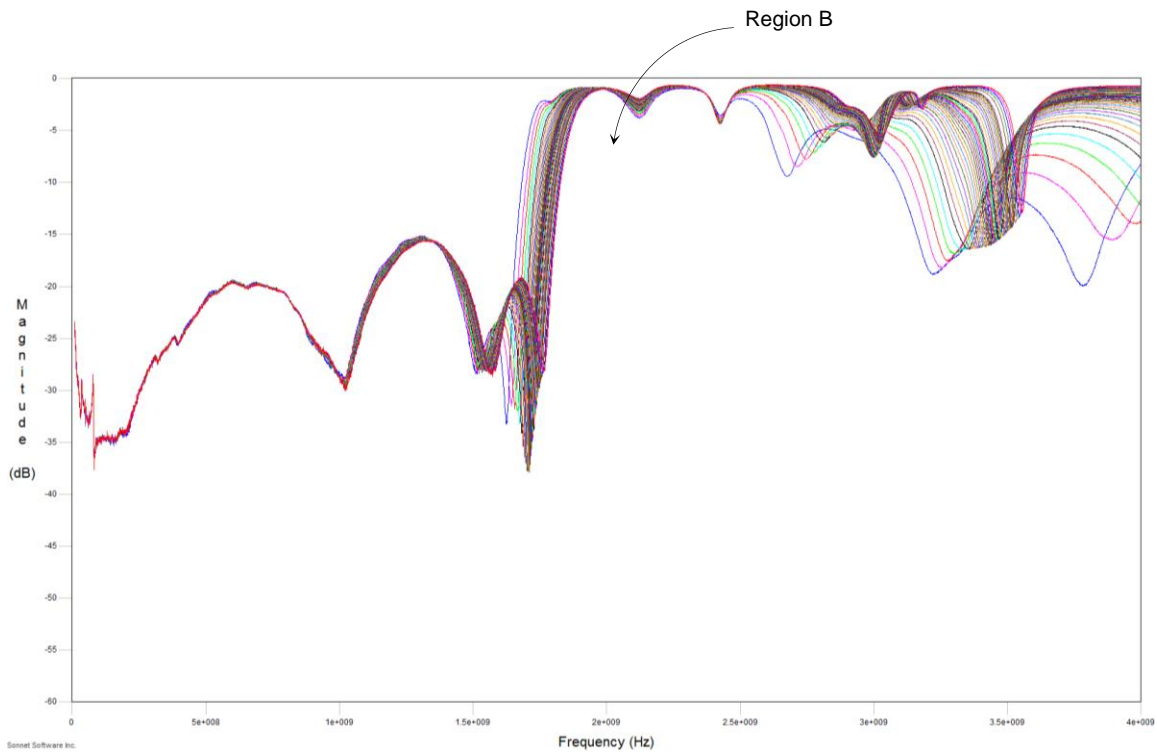
Figure 3.18 Measured tuning range of the right sub-filter in Figure 3.14 from 0 V to 20 V

The measured results of the structure shown in Figure 3.16 are presented in Figure 3.19. As can be seen, this filter has a relatively constant bandwidth of 100 MHz over the tuning range. The insertion loss ranges from 5 dB to 6 dB within the tunable passband without metallic housing. Compared to the bandwidth in Figure 3.15 (which is around a 3-dB bandwidth of 300 MHz), the response in Figure 3.19 has a bandwidth one-third of Figure 3.15, whereas the insertion loss has only increased by a factor of two. This is an improvement on the Q factor compared to using traditional filter synthesis because the traditional approach will increase the insertion loss by an approximate factor of three if the bandwidth is reduced to one-third.
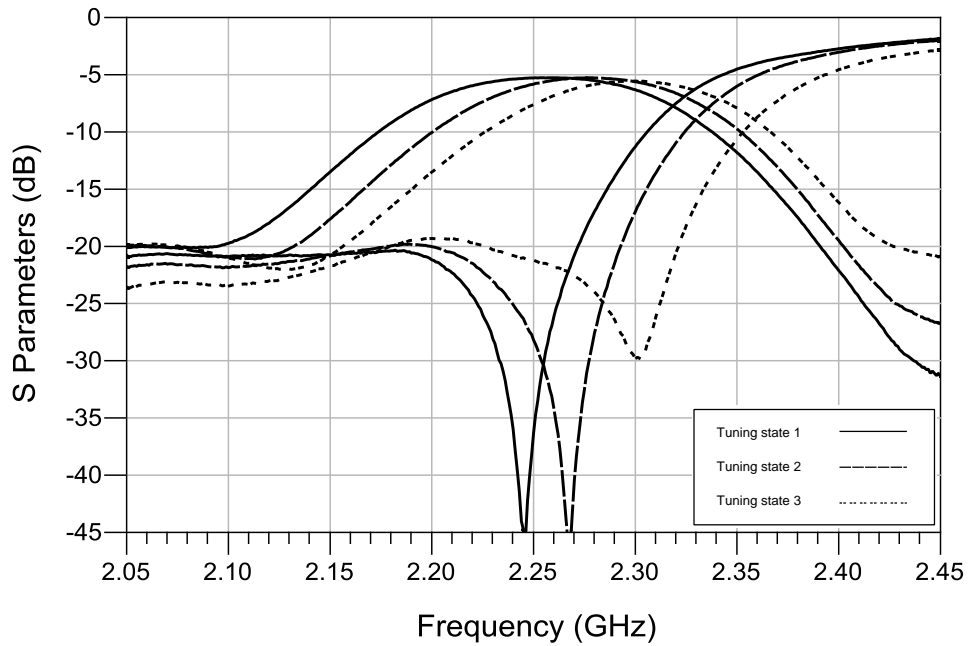
Figure 3.19 Measured results for the tunable band-pass filter with two identical band-stop filters

Chapter 4

Concepts of Performance Improvements

4.1 Introduction

This chapter illustrates several additional concepts for improving the performance of the tunable band-pass filter described in Chapter 3. These concepts include substituting sub-filters with lossy filters, and pre-optimizing the sub-filters. At the end of the chapter, we present a conceptual model of a diplexer employing two band-pass filters.

4.2 Substituting the Second Sub-filters with Lossy Filters

The first concept proposed is taking advantage of the fact that the return loss of a lossy filter can have a sharp roll-off on the edge of the passband while sacrificing the insertion loss in the passband [37-38]. The second sub-filter, which provides Region B described in Chapter 3, can be replaced by one of these lossy filters to further improve the sharpness of the low-frequency band edge.

   A typical lossy filter structure and its response are shown in Figure 4.1. Figure 4.1 (a) illustrates a block diagram of a lossy filter F1, and Figure 4.1 (b) shows an equivalent schematic structure of the lossy filter using F2 as a standard (non-lossy) filter; and two attenuators A1 and A2 (3dB as an example), respectively. The simulated response of this lossy filter has 6dB loss in both transmission and reflection, as shown in Figure 4.1 (c).

(a)

(b)

f2
dB(S(1,1))=-6.000

f1
dB(S(2,1))=-6.000
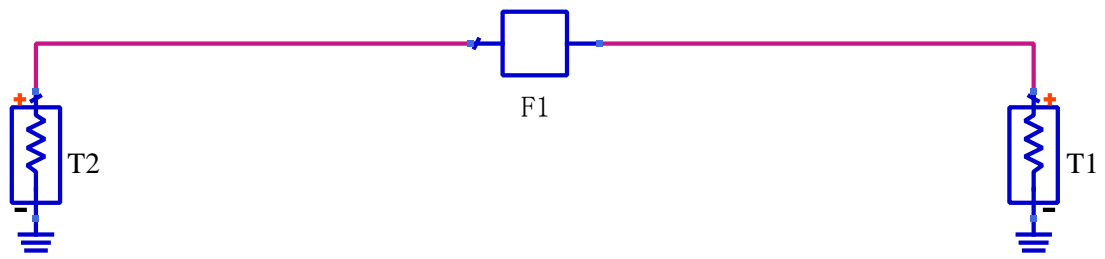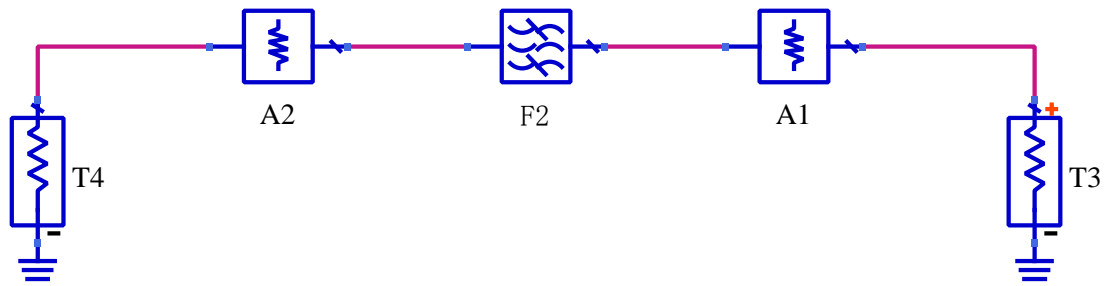
Region B
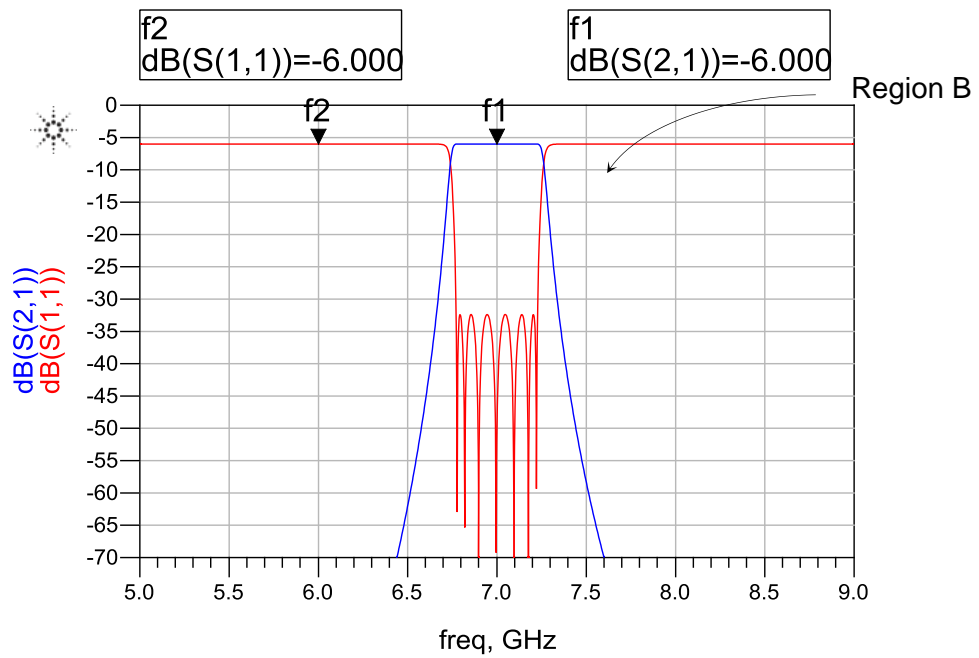
(c)

Figure 4.1 (a) a lossy filter, (b) representation of the lossy filter using an ideal filter and two attenuators, (c) response of the lossy filter

29

In order to get a sharp roll-off on the edge of the passband for the return loss, attenuators should only be added at the output port. Figure 4.2 shows the structure and response of this variation of a lossy filter. Figures 4.2 (a) and (b) show the block diagram of a lossy filter and its equivalent schematic structure, respectively. Filter F2 is a standard (non-lossy) filter. A 3dB attenuator, A1, connects between F2 and the output port, T4. Figure 4.2 (c) presents the simulated response of this structure. The graph shows a 3dB insertion loss due to the attenuator at the output, but there is no loss in the reflected signal. Hence, it effectively forms a sharp roll-off for the return loss on the edge of the passband.

Moreover, a 3dB insertion loss in the passband of the second sub-filter does not affect the final response of the resultant filter because only Region B, as shown in Figure 4.2 (b), is used in constructing the resultant filter. Therefore, the insertion loss can be sacrificed for a sharp roll-off for the return loss on the band edge.
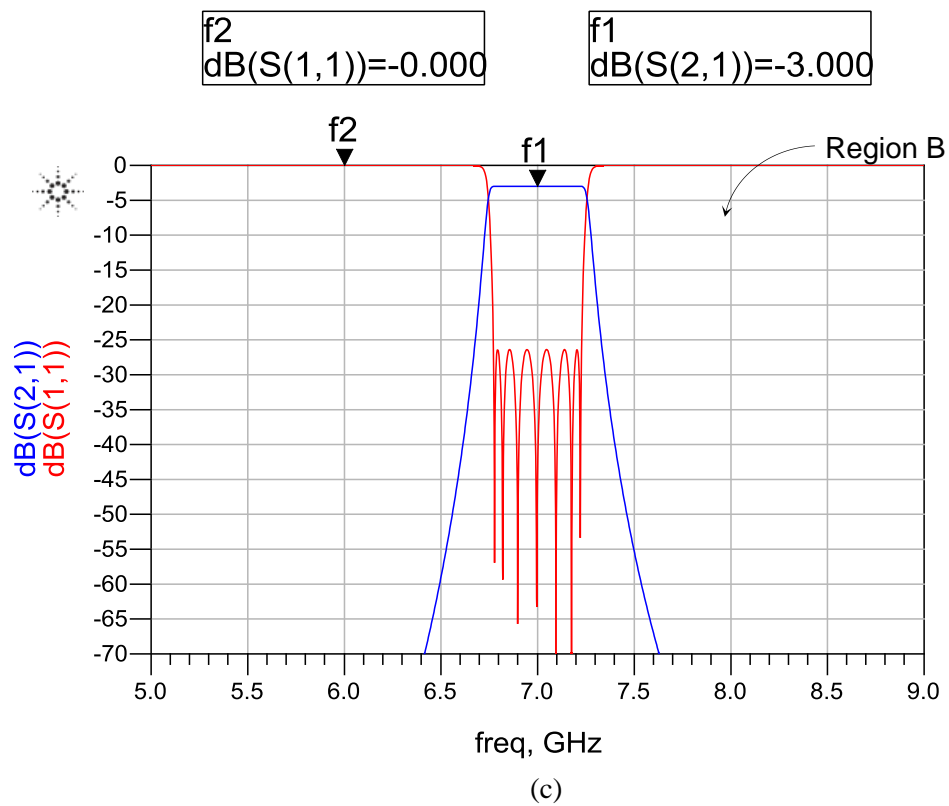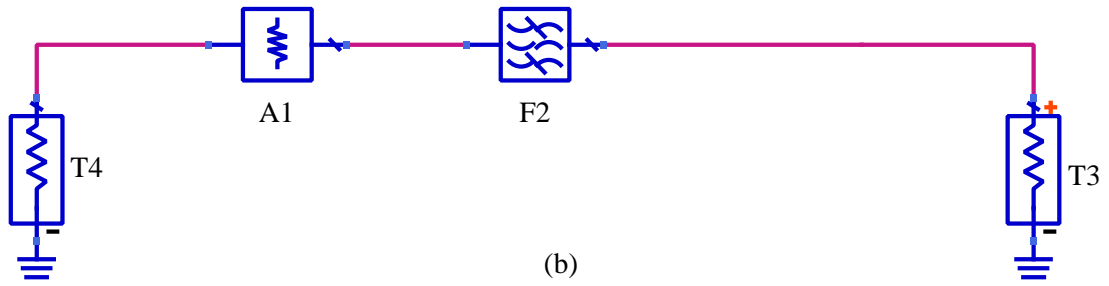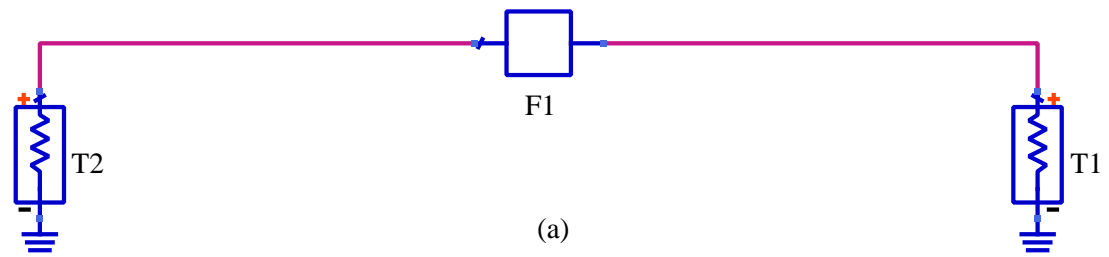
Figure 4.2 (a) variation of a lossy filter, (b) representation of the lossy filter using an ideal filter and an attenuator, (c) response of the lossy filter

Figure 4.3(a) shows a proposed band-pass filter structure with a lossy filter as one of its sub-filters. F1 is standard (non-lossy) band-pass sub-filters, F2 is a lossy band-pass sub-filter as described in Figure 4.2, and C1 is a counter-clockwise circulator. T1 and T2 are the input and output port of the system, respectively. T3 is a 50-Ω termination at the output port of F2. Figure 4.4(b) is a signal flow chart for this filter structure. Note that the signal flow is very similar to the process described in Figure 3.2, except that the sub-filters employed here are band-pass sub-filters.

(a)   (b)
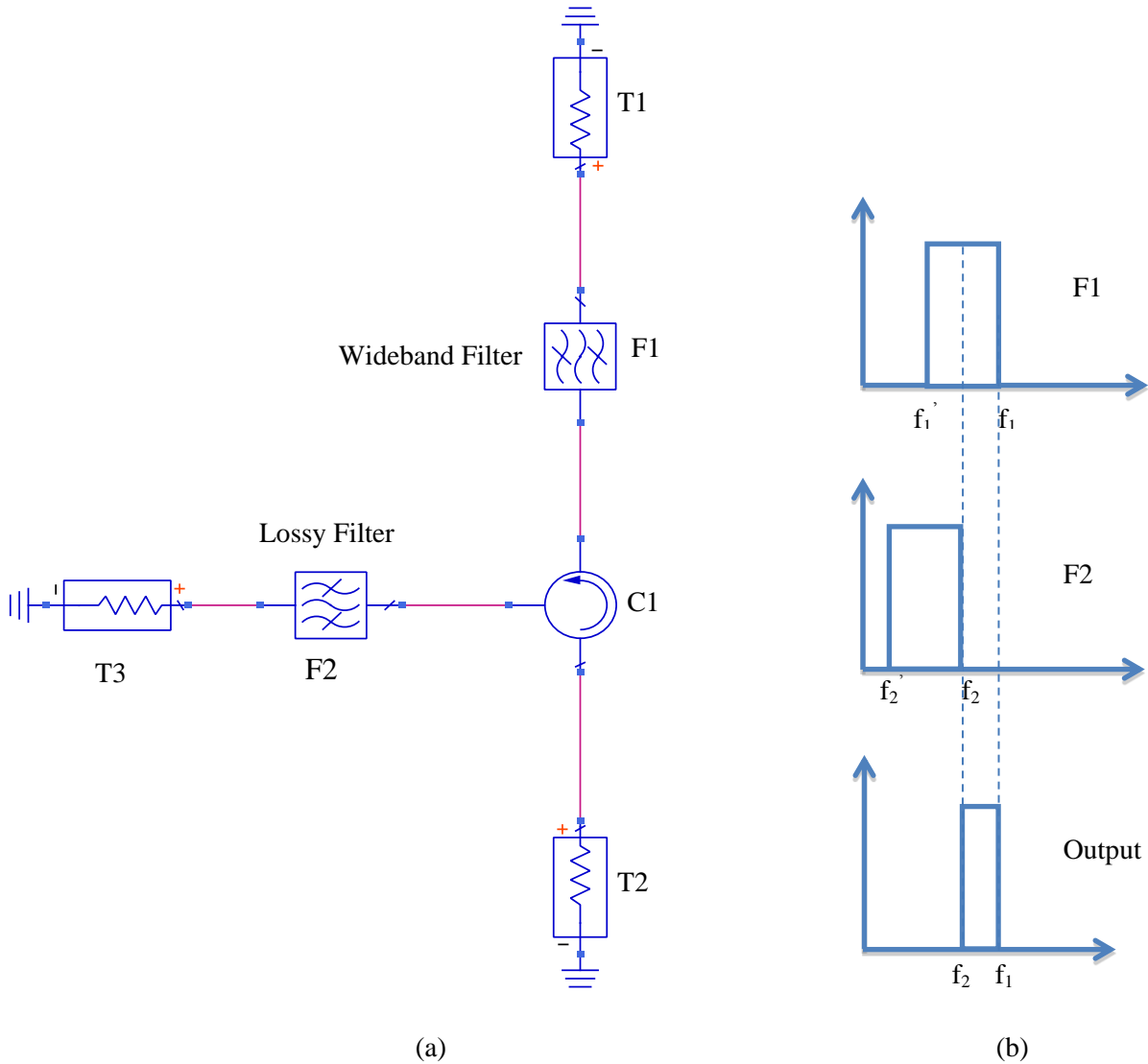
Figure 4.3 Graphs of (a) the proposed band-pass filter structure with a wideband filter (F1) and a lossy filter (F2) and (b) a sketch of its responses

Figure 4.4 shows the circuit simulation results for the structure proposed in Figure 4.3. Figure 4.4 (a) is the response of a wideband band-pass sub-filter, which represents F1 in the system of Figure 4.3 (a). Figure 4.4 (b) is the response of a lossy filter, which represents F2 in the system of Figure 4.3. Figure 4.4 (c) shows the reflection at the input port of the lossy filter in Figure 4.4 (b), with a 50-Ω termination. Figure 4.4 (d) presents the final output of the proposed filter structure in Figure 4.3. Figure 4.4 (e) is the zoomed-in view of the response in Figure 4.4 (d).

It can be seen that the insertion loss has a very sharp roll-off at the left edge of the passband of the constructed filter in Figure 4.4 (e) after lossy filter is introduced.
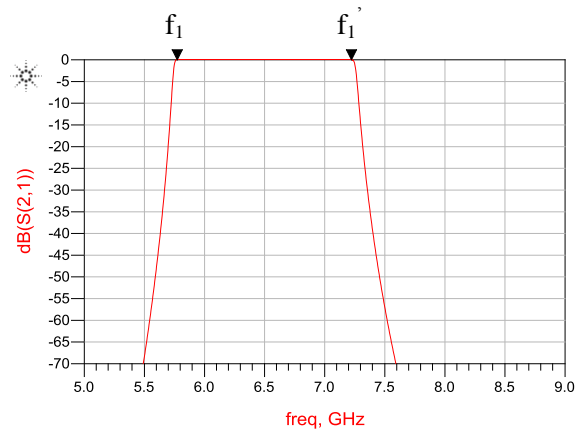
(a)
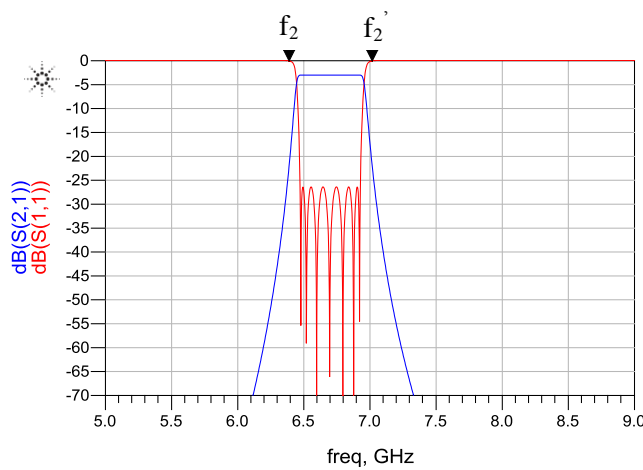
(b)
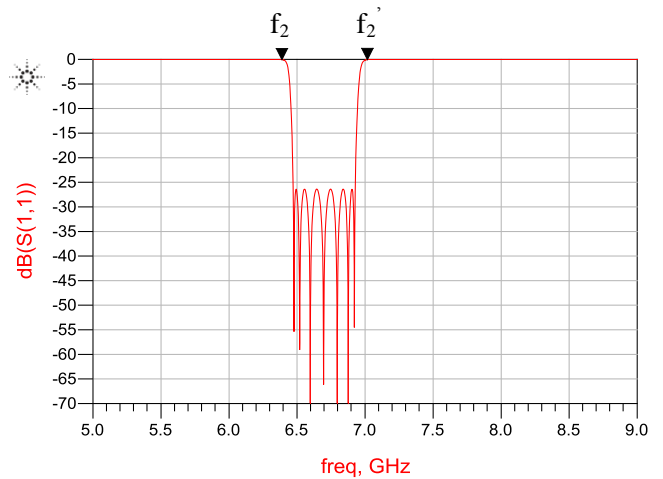
(c)
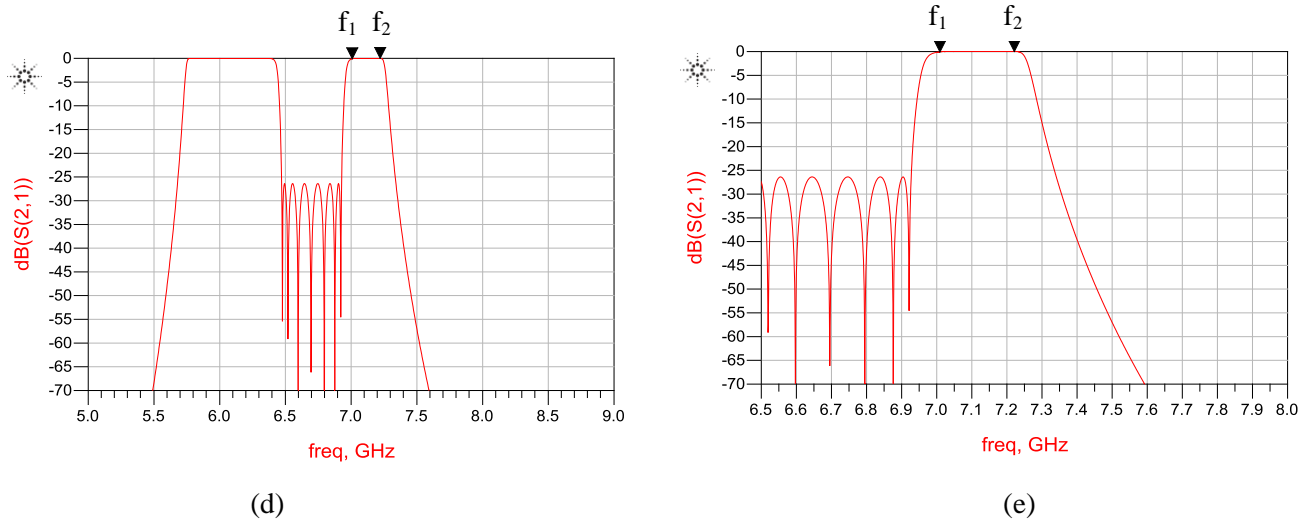
Figure 4.4 Circuit simulation results of a band-pass filter structure with one wideband band-pass sub-filter and one lossy bandpass sub-filter, as proposed in Figure 4.3

4.3 Pre-optimizing Sub-filters

The second proposed concept for improving the performance of the band-pass filter is pre-optimizing the sub-filters. This section demonstrates how pre-optimization works by comparing the responses of a standard sub-filter and a pre-optimized sub-filter.

Figure 4.5 employs a pre-optimized wideband band-pass filter and a lossy band-pass sub-filter to build the system depicted in Figure 4.3. Figure 4.5 (a) shows the standard response of a five-pole wideband band-pass sub-filter with both notches on the right-hand side to improve rejection in the higher frequency band as well as to achieve a sharper roll-off for its insertion loss on the right edge of the passband. Figure 4.5 (b) presents the pre-optimized response of the filter in Figure 4.5 (a). It is pre-optimized in such a way that the desired band of the final output (between f1 and f2) is tuned to have a higher return loss and correspondingly a lower insertion loss than the standard response. However, the rest of the band (between f1$^{'}$ and f2) is sacrificed and shows lower return loss. In the meantime, the band between f3 and f3$^{'}$ is also pre-optimized to have a higher rejection than the standard response. Figure 4.5 (c) shows the response of the lossy sub-filter depicted in Figure 4.2. Figure 4.5 (d) presents the resultant final output.

The final response in Figure 4.5 (d) demonstrates that the filter constructed from a pre-optimized sub-filter and a lossy sub-filter has an extremely high return loss of 45dB and a very sharp roll-off on

both edges of the passband. It should be noted that this pre-optimization approach can also be applied to the second sub-filter, which is the lossy filter, to achieve an even better performance in the final output.
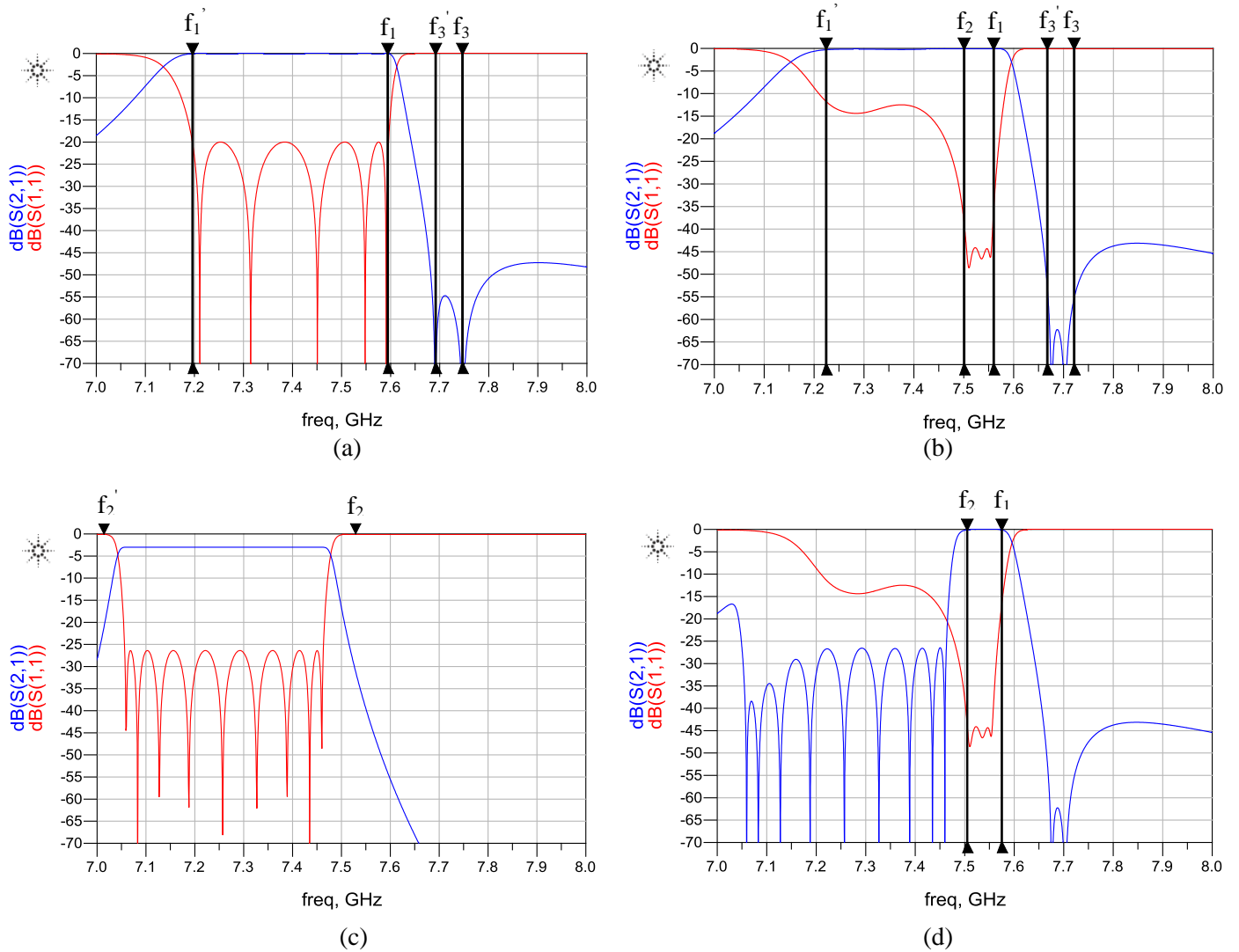
Figure 4.5 Responses of the band-pass filter proposed in Figure 4.3 incorporating pre-optimized sub-filter and a lossy sub-filter, along with its responses

4.4 Doubling the Second Sub-filter

The third proposed concept for improving the performance of the band-pass filter is integrating into the structure a third sub-filter which is identical to the second sub-filter. This section illustrates this concept and demonstrates the improvement of out-of-band rejection from applying this approach.

Figure 4.6 shows the proposed band-pass filter structure. F1, F2 and F3 are three tunable band-pass sub-filters, F2 and F3 are two identical sub-filters, C1 and C2 are two counter-clockwise circulators, T1 and T2 are the input and output port of the system, respectively, and T3 and T4 are two 50-Ω terminations at the output port of F2 and F3, respectively. F3 is used in conjunction with F2 to enhance out-of-band rejection. The signal coming out of the bottom of C1 will be the same as the last graph shown in Figure 4.3. When this signal goes through the F3 branch, the signal between f1 and f2 will be attenuated again by the return loss of F3, thereby improving the lower-frequency rejection for the output signal at T2.
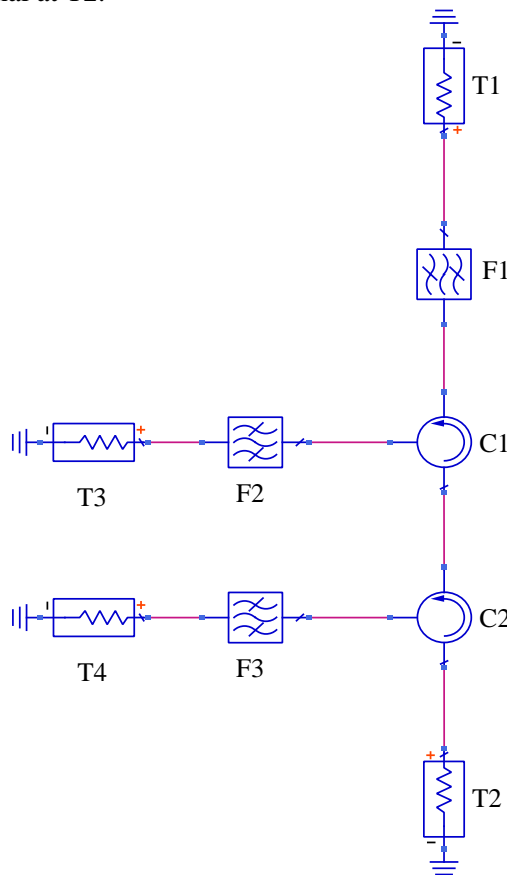
Figure 4.6 Graphs of another proposed band-pass filter structure with three band-pass sub-filters, two of which are used in conjunction to enhance out-of-band rejection

36

Figure 4.7 shows graphs of simulated responses for the structure proposed in Figure 4.6. Figure 4.7 (a) is the response of a wideband band-pass sub-filter, which represents F1 in the system of Figure 4.6. Figure 4.7 (b) is the response of a lossy filter, which represents both F2 and F3 in the system of Figure 4.6. Figure 4.7 (c) shows the reflection at the input port of a lossy filter in Figure 4.6 with a 50-Ω termination. Figure 4.7 (d) presents the final output of the proposed filter structure in Figure 4.6. Figure 4.7 (e) is the zoomed-in view of the response in Figure 4.4 (d).

By comparing Figure 4.7 (e) and Figure 4.4 (e), one can observe that the lower-frequency rejection has improved from -26dB to -52dB.

(a)

(b)

(c)
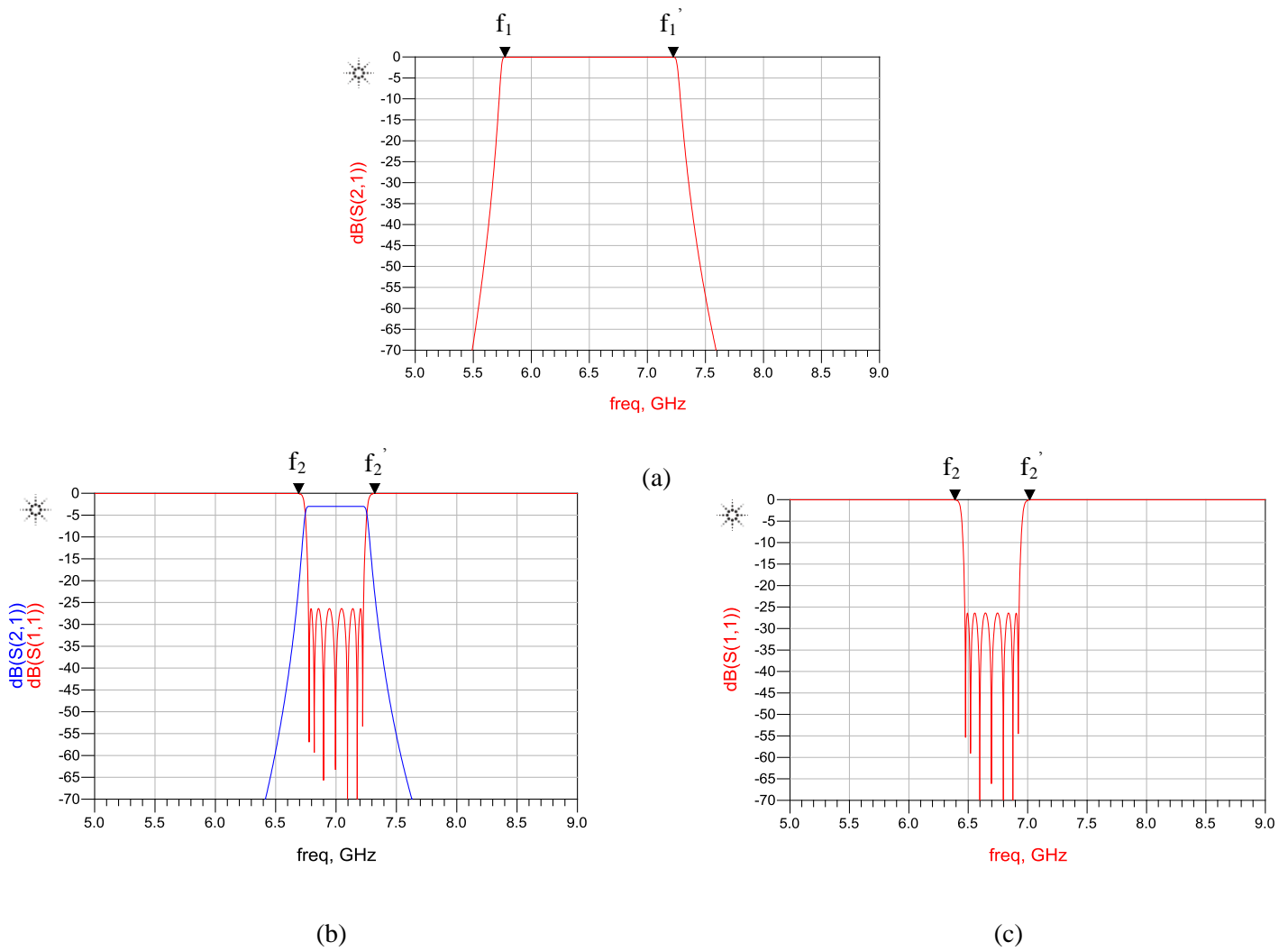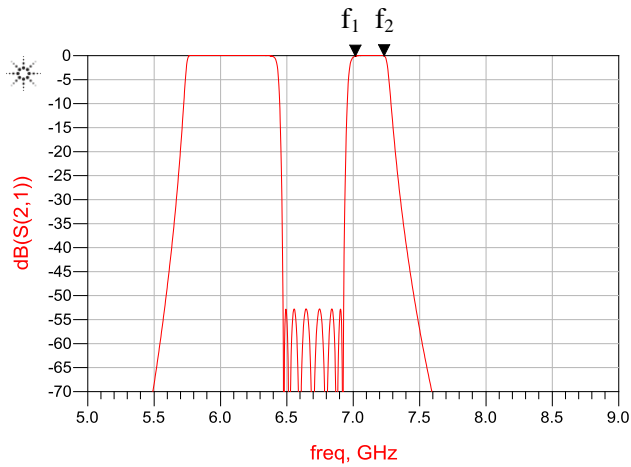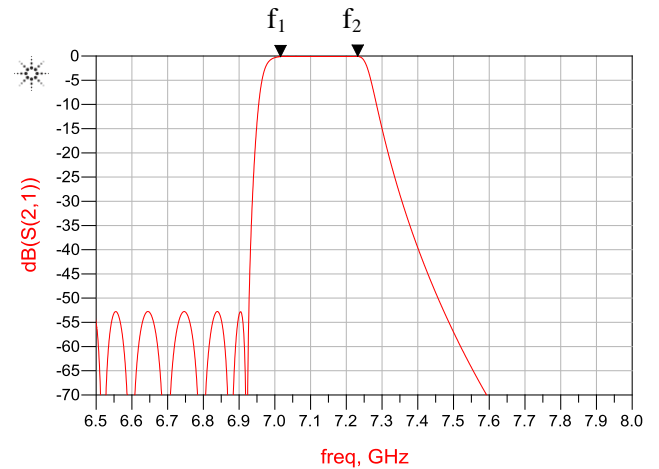
Figure 4.7 Circuit simulation results of band-pass filter structure with one wideband band-pass sub-filter and two lossy band-pass sub-filters, as proposed in Figure 4.6

4.5 Two Pre-optimized Band-stop Filters

Another possible concept for improving the performance of the band-pass filter is using two band-stop sub-filters that are pre-optimized at the band edges.

Figure 4.8 (a) shows the proposed band-pass filter structure. F1 and F2 are two band-stop sub-filters, where F1 is pre-optimized to provide a sharp cut-off at f1 where as F2 is pre-optimized to provide a sharp cut-off at f2. Figure 4.6 (b) presents the final response at the output of the system shown in Figure 4.8 (a). The band between f1 and f2 forms the passband of a band-pass filter.

(a)

(b)
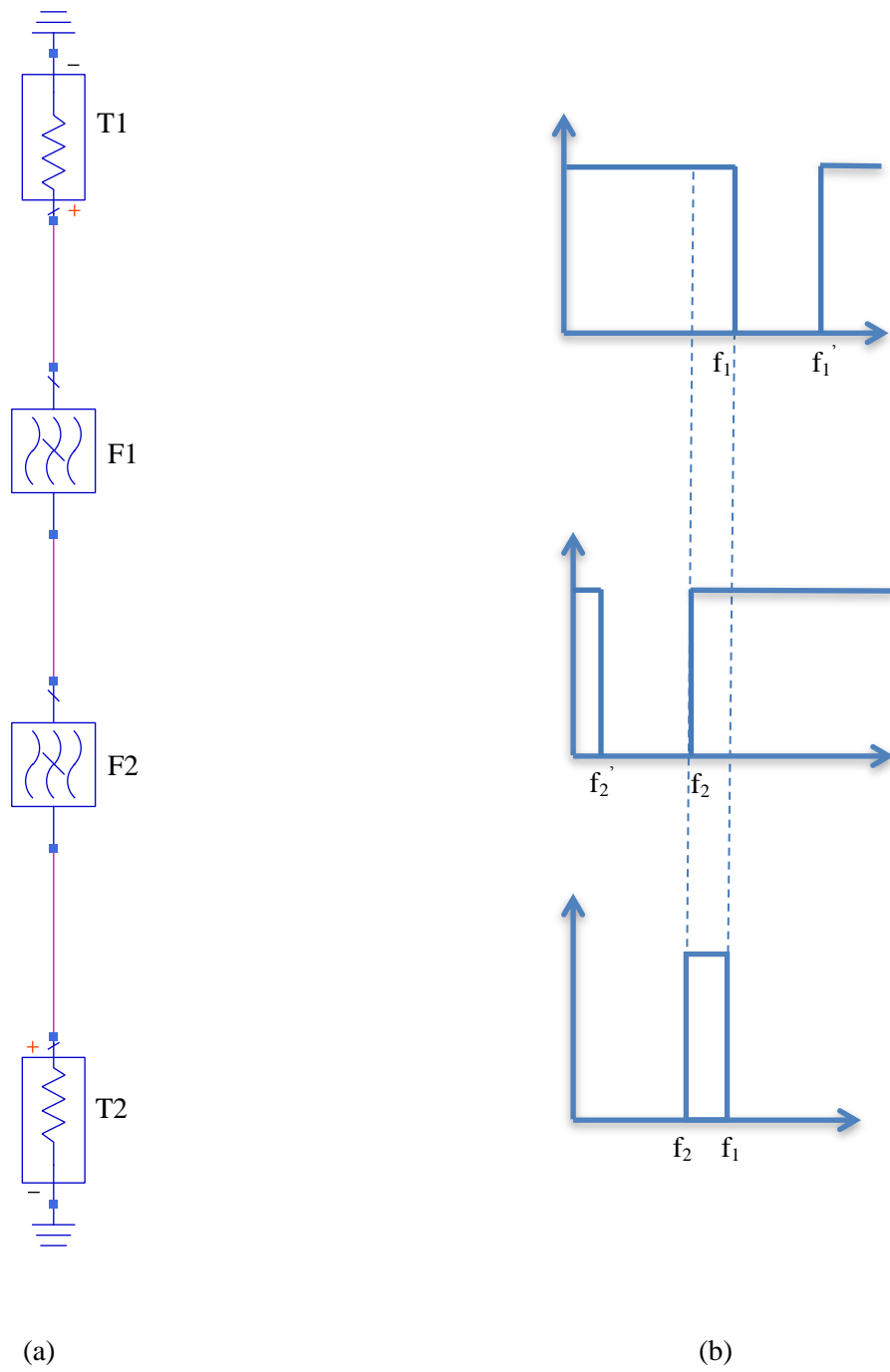
Figure 4.8 Graphs of (a) the proposed band-pass filter structure with two band-stop sub-filters and (b) a sketch of its theoretical response

Figure 4.9 shows circuit simulation results for the structure proposed in Figure 4.8. Figure 4.9 (a) is the response of a band-stop sub-filter, which represents F1 in the system of Figure 4.8. Figure 4.9 (b) is the response of another band-stop filter, which represents F2 in the system of Figure 4.8. Figure 4.9 (c) presents the final output of the proposed filter structure in Figure 4.8. Figure 4.9 (d) is the zoomed-in view of Figure 4.9 (c).

In addition, similar to the approach in Figure 4.5, one can incorporate pre-optimized tunable band-stop sub-filters to make this band-pass filter tunable.

(a)

(b)

(c)   (d)
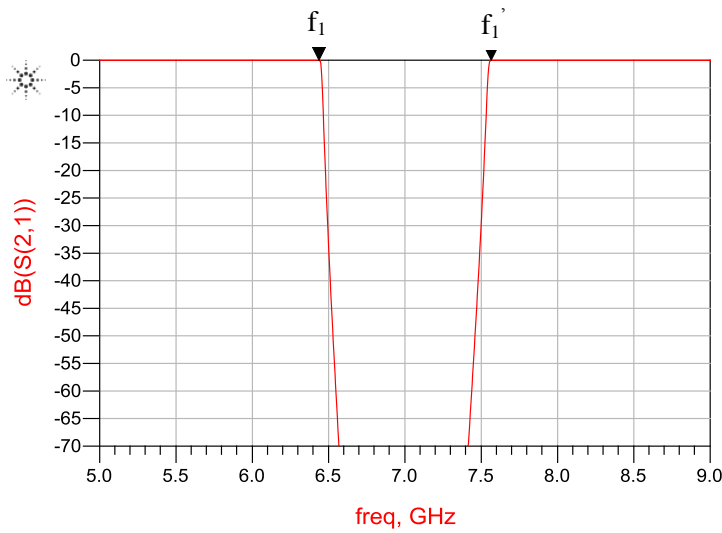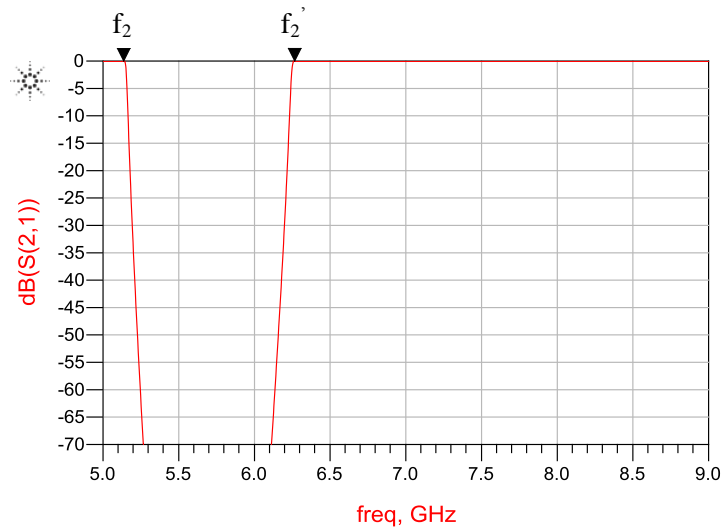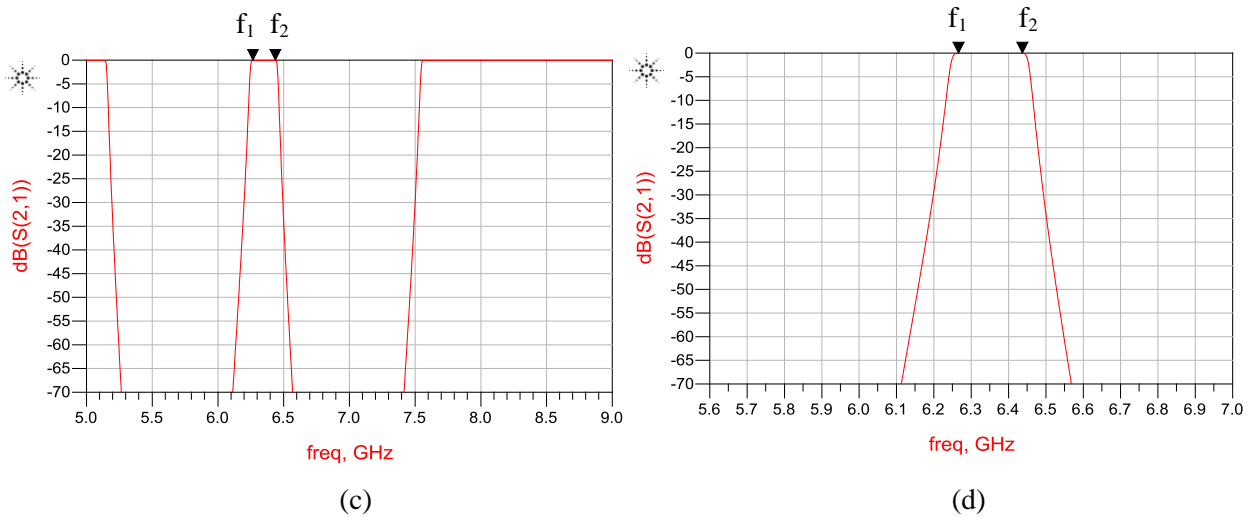
Figure 4.9 Circuit simulation results of the proposed band-pass filter structure with two band-stop sub-filters

4.6 A Conceptual Model of a Diplexer

The previous sections in this chapter illustrated four approaches for improving the performance of the band-pass filter proposed in Chapter 3. However, the discussions revolved around the framework of one single band-stop filter. The potential of constructing a diplexer by using two of these band-stop filters has not been discussed. In this section, a conceptual model of a diplexer is proposed to integrate two of these band-stop filters to achieve a high-Q diplexer with tunability.

Figure 4.10 shows a diplexer structure constructed from two of the proposed tunable band-stop filters presented in Figure 3.3. C1 and C2 are two counter-clockwise circulators, C3 is a clockwise circulator, F1 and F2 are two band-stop sub-filters designated for the lower frequency band of the diplexer, F3 and F4 are two band-stop sub-filters designated for the higher frequency band of the diplexer, T1 is the input port of the system, T2 and T3 are the two output port of the diplexer, and T4 and T5 are two 50-Ω terminations at the output port of F2 and F4, respectively. The signal propagates from T1 into C1, moves in a counter-clockwise direction, and then enters the left channel, which starts with F1 and has an output band from f1 to f2. Since only a portion of the initial signal (between f1 and f1') is propagated through filter F1, the rest of the signal gets reflected by F1. It re-enters C1, which directs the signal counter-clockwise into the right channel of the diplexer; it then starts with F3

41

and has an output band from f3 to f4. Therefore, the signal output from T2 combines with the signal output from T3 to form the final output of this diplexer structure. It should be noted the approaches presented in the previous sections for the sub-filters can be also employed to improve the overall performance of the diplexer.
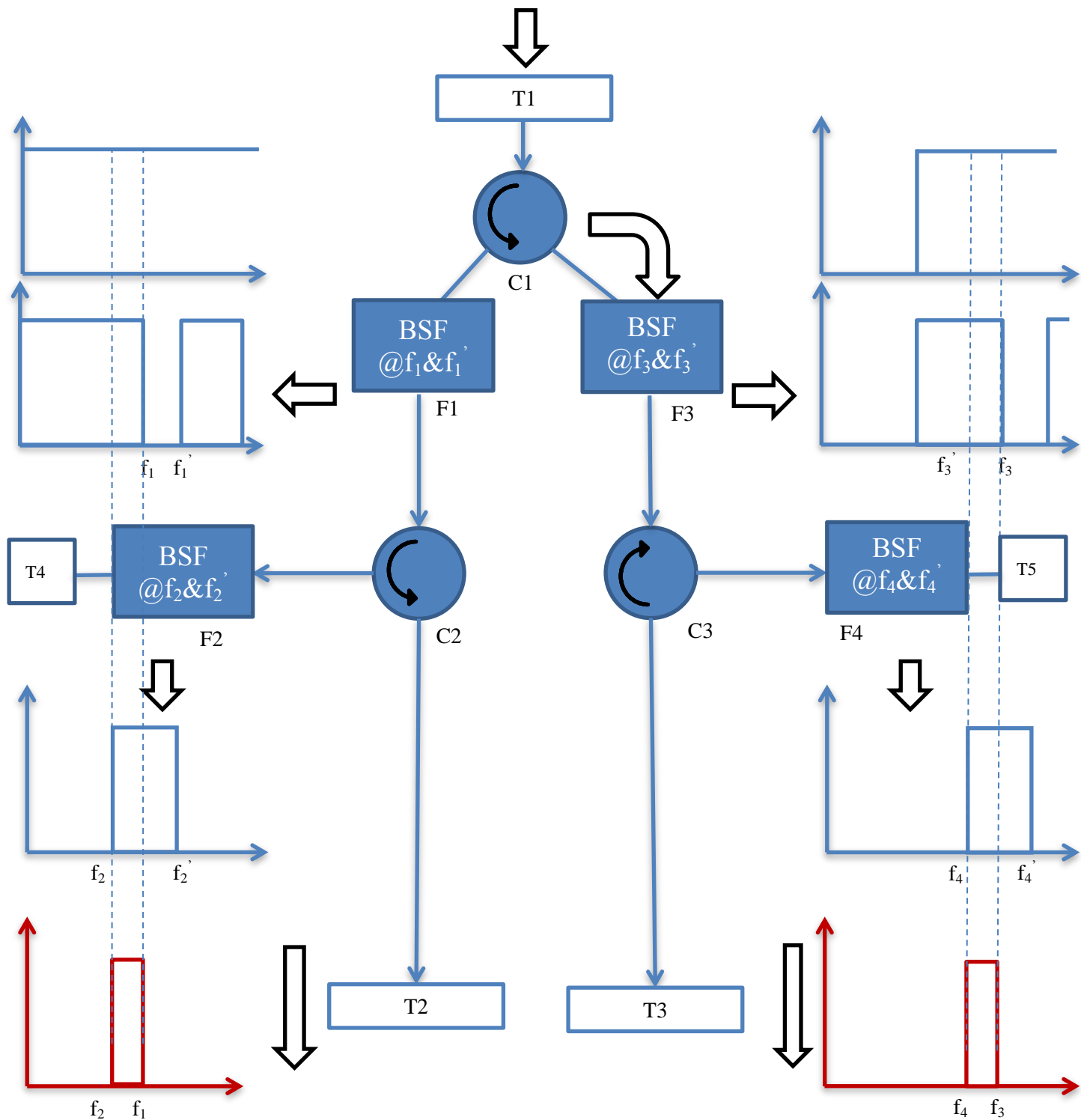
Figure 4.10 A chart of diplexer structure comprised of two of the proposed band-stop filters as in Figure 3.3

Figure 4.12 shows the ADS circuit simulation results of the proposed diplexer with two band-pass sub-filters. Channel 1 corresponds to the left branch of the structure in Figure 4.10, and channel 2 corresponds to the right branch of the structure in Figure 4.10.
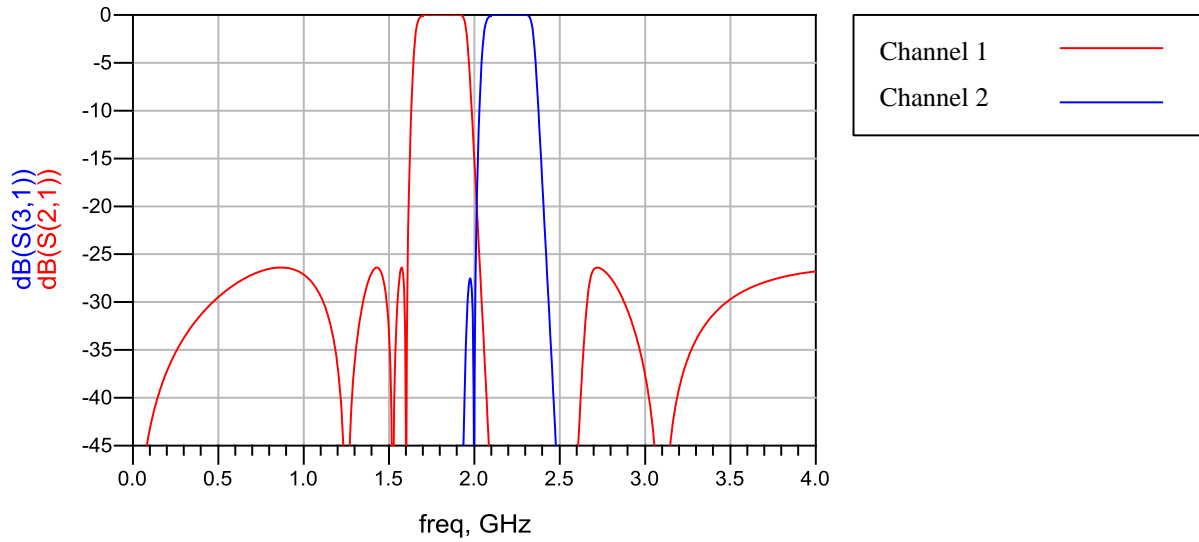
Figure 4.11 Circuit simulation responses of the proposed diplexer structure with two band-pass sub-filters

Figure 4.12 shows the Sonnet EM simulation results of the proposed diplexer. Channel 1 is the output of the left branch of the structure in Figure 4.10, and channel 2 is the output of the right branch. The diplexer can be made tunable by integrating varactors in slot of the band-stop filter shown in Figure 3.3.
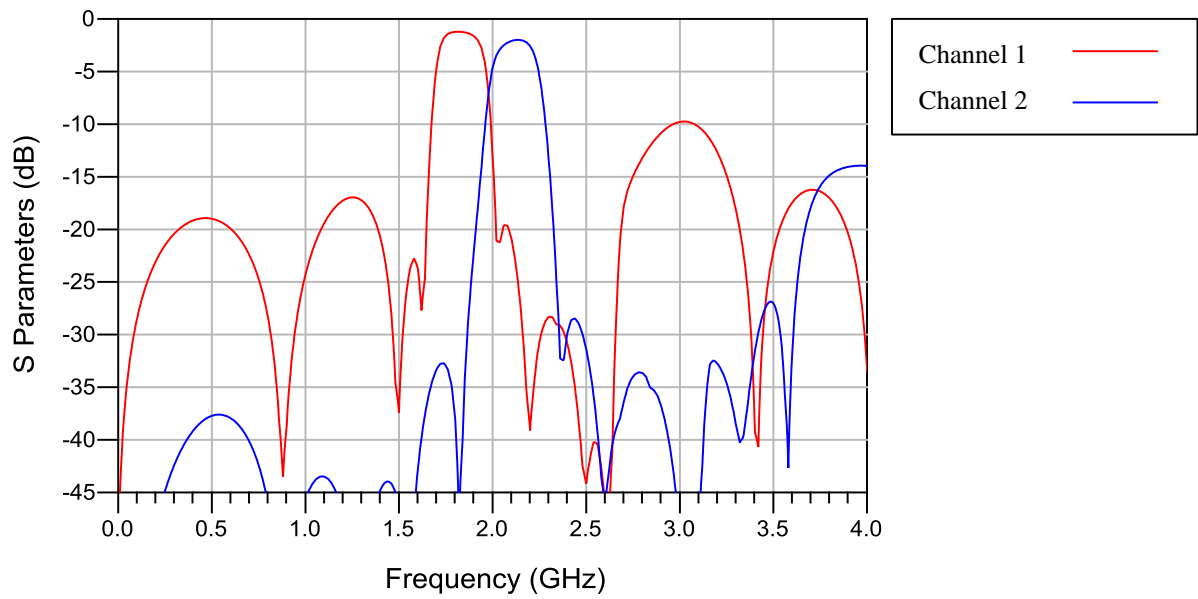
Figure 4.12 EM simulation results of a tunable diplexer with MA46603-134 varactors on a Rogers RO3210 substrate

Chapter 5

Conclusion

5.1 Contributions

The primary contributions of this thesis are as follows:

- A novel way was presented to design a tunable band-pass filter using two band-stop filters.

This thesis presented an alternative approach for constructing a tunable band-pass filter using two band-stop filters and a circulator. Such a structure is capable of achieving a tunable filter both in center frequency and bandwidth, including the realization of tunable filters with a constant absolute bandwidth. The measured results show good tunability and relatively constant bandwidth. The loss is relatively small due to having used two wideband band-stop subfilters. The proposed structure can be easily implemented, since it requires only the use of tuning elements for the resonators.

- Several concepts were described for improving the performance of the aforementioned constructed band-pass filter.

This thesis also presented four approaches for further improving the band-pass filter constructed using two band-stop filters and a circulator. These concepts include substituting the second sub-filter in the structure with a lossy filter to improve edge roll-off, pre-optimizing the sub-filters prior to integration to increase the Q factor, introducing a third sub-filter that is identical to the second sub-filter after the second sub-filter to improve rejection, and constructing band-pass using two pre-optimized band-stop filters.

- A new approach was provided for constructing a tunable diplexer.

A tunable diplexer was constructed in this thesis using four sub-filters and three circulators. The conceptual diplexer was presented with a flow chart. These four sub-filters can be made tunable and can be optimized using previous optimization methods to make this diplexer a high-Q tunable diplexer. In addition, a diplexer with MA46603-134 varactors on a Rogers RO3210 substrate was simulated using EM simulation software Sonnet.

5.2 Future Work

Despite the several contributions explained above, the band-pass filter still reveals relatively high insertion loss. A portion of this loss is attributed to radiation, since the filter is not packaged in a metallic box. With the use of packaging and a low-loss circulator design, a much better insertion loss performance can be potentially achieved.

It should also be noted that the measurement results of the band-pass filter in Chapter 3 are obtained by applying the same DC bias voltage to all four varactors on a sub-filter. A much better performance can be achieved through non-synchronous tuning, where the DC bias voltages for the varactors are tuned to optimize the overall filter performance.

In addition, the concepts of performance improvements illustrated in Chapter 4 have only been demonstrated in simulations. Future work is needed to further verify these improvements experimentally with fabricated devices. Moreover, other approaches, such as optimizing the coupling matrix of individual sub-filters, can further improve the performance of the band-pass filter.

Bibliography

[1] S. R. Chandler, I. C. Hunter, and J. G. Gardiner, "Active varactor tunable bandpass filter," *IEEE Microwave Guided Wave Lett.*, vol. 3, no. 3, pp. 70–71, Mar. 1993.

[2] A. R. Brown and G. M. Rebeiz, "A varactor-tuned RF filter," *IEEE Trans. Microwave Theory Tech.*, vol. 48, no. 7, pp. 1157–1160, July 2000.

[3] G. Torregrosa-Penalva, G. Lopez-Risueno, and J. I. Alonso, "A simple method to design wide-band electronically tunable combline filters," *IEEE Trans. Microwave Theory Tech.*, vol. 50, no. 1, pp. 172–177, Jan. 2002.

[4] A. Tombak, F. T. Ayguavives, J.-P. Maria, G. T. Stauf, A. I. Kingon, and A. Mortazawi, "Tunable RF filters using thin film barium strontium titanate based capacitors," *IEEE MTT-S Int. Microwave Symp*. Dig., 2001, vol. 3, pp. 1453–1456.

[5] B. H. Moeckly and Y. Zhang, "Strontium titanate thin films for tunable YBa2Cu3O7 microwave filters," *IEEE Trans. Appl. Superconduct.*, vol. 11, no. 1, pp. 450–453, Mar. 2001.

[6] F. Kuttner, "YIG tracking filters expands dynamic range of spectrum analyzers," *Microwave System News*, May 1987.

[7] M. Tsutsumi and K. Okubo, "On the YIG film filters," *IEEE MTT-S Int. Microwave Symp. Dig.*, June 1992, vol. 3, pp. 1397–1400.

[8] J. Uher, F. Arnot, and J. Bornrmann, "Computer aided design and improved performance of tunable ferrite-loaded E-plane filters," *IEEE Trans. Microwave Theory Tech.*, vol. 36, no. 5, pp. 1841–1849, Dec. 1988.

[9] T.-Y. Yun and K. Chang, "Piezoelectric-transducer-controlled tunable microwave circuits," *IEEE Trans. Microwave Theory Tech.*, vol. 50, no. 5, pp. 1303–1310, May 2002.

[10] A. Abbaspour-Tamijani, L. Dussopt, and G. M. Rebeiz, "Miniature and tunable filters using MEMS capacitors," *IEEE Trans. Microwave Theory Tech.*, vol. 51, no. 7, pp. 1878–1885, July 2003.

[11] G. Rebeiz and C. Goldsmith, "WMB: MEMS, BAW, and micromachined filter technology," *Proc. 2004 IEEE MTT-S Int. Microwave Symp. Dig.,* IMS Workshop, June 2004, pp. 12–13.

[12]   R. R. Mansour, "High Q MEMS tunable filters," *Proc. IEEE IMS Workshopon High-Q RF MEMS Tunable Filters,* June 2007.

[13]   M. Sterns, M. Hrobak, S. Martius and L. -. Schmidt, "Magnetically tunable filter from 72 GHz to 95 GHz," *German Microwave Conference*, 2010, 2010, pp. 82-85.

[14]   B. K. Kuanr, V. Veerakumar, K. Lingam, S. R. Mishra, A. V. Kuanr, R. E. Camley and Z. Celinski, "Microstrip-Tunable Band-Pass Filter Using Ferrite (Nanoparticles) Coupled Lines," *Magnetics, IEEE Transactions on*, vol. 45, pp. 4226-4229, 2009. 139

[15]   Zhou Hao-Miao, Xia Zhe-Lei and Deng Juan-Hu, "The research of dual-tunable magnetoelectric microwave filters: Numerical simulation of the magnetoelectric microwave filters based on theoretical model of electric tuning ferromagnetic resonance," *Communications and Mobile Computing (CMC),* 2011 Third International Conference on, 2011, pp. 258-261.

[16]   C. S. Tsai, G. Qiu, H. Gao, L. W. Yang, G. P. Li, S. A. Nikitov and Y. Gulyaev, "Tunable wideband microwave band-stop and band-pass filters using YIG/GGG-GaAs layer structures," *Magnetics, IEEE Transactions on*, vol. 41, pp. 3568-3570, 2005.

[17]   J. Clarke and M. R. B. Dunsmore, "High-power tunable YIG filters," *Microwaves, Antennas and Propagation, IEE Proceedings H*, vol. 132, pp. 251-254, 1985.

[18]   W. Keane, "Narrow-band YIG filters aid wide-open receivers," *Microwaves,* vol. 17, pp. 50–54, 1978.

[19]   J. Krupka, A. Abramowicz and K. Derzakowski, "Magnetically tunable filters for cellular communication terminals," *Microwave Theory and Techniques, IEEE Transactions on,* vol. 54, pp. 2329-2335, 2006.

[20]   A. Tombak, J.-P. Maria, F. T. Ayguavives, Z. Jin, G. T. Stauf, A. I. Kingon, and A. Mortazawi, "Voltage-controlled RF filters employing thin-film barium-strontium-titanate tunable capacitors," *IEEE Trans. Microwave Theory & Tech*., vol. 51, no. 2, pp. 462–467, Feb. 2003.

[21]   K. B. Kim, "Tunable dual-mode filter using varactor and variable ring resonator on integrated BST/TiO2/Si substrate," *Electronics Letters*, vol. 46, pp. 509-511, 2010. 138

[22]   Young-Hoon Chun, Jia-Sheng Hong, P. Bao, T. J. Jackson and M. J. Lancaster, "BST-varactor tunable dual-mode filter using variable ZC transmission line," *IEEE Microwave and Wireless Components Letters,* vol. 18, pp. 167-9, 03, 2008.

[23]   Ken Zhang, T. Watson, A. Cardona and M. Fink, "BaSrTiO3-based 30–88MHz tunable filter," *Microwave Symposium Digest (MTT),* 2010 IEEE MTT-S International, 2010, pp. 1492-1495.

[24]   J. Nath, D. Ghosh, J. -. Maria, A. I. Kingon, W. Fathelbab, P. D. Franzon and M. B. Steer, "An electronically tunable microstrip bandpass filter using thin-film Barium-Strontium-Titanate (BST) varactors," *Microwave Theory and Techniques, IEEE Transactions on*, vol. 53, pp. 2707-2712, 2005.

[25]   D. Kuylenstierna, A. Vorobiev and S. Gevorgian, "40 GHz lumped element tunable bandpass filters with transmission zeros based on thin Ba/sup 0.25/Sr/sup 0.75/TiO/sup 3/ (BST) film varactors," *Silicon Monolithic Integrated Circuits in RF Systems*, 2006. Digest of Papers. 2006 Topical Meeting on, 2006, pp. 4 pp.

[26]   Young-Hoon Chun, Jia-Sheng Hong, Peng Bao, T. J. Jackson and M. J. Lancaster, "Tunable bandstop filters using BST varactor chips," *Microwave Conference*, 2007. European, 2007, pp. 110-113.

[27]   Y. Chun, H. Shaman and J. Hong, "Switchable embedded notch structure for UWB bandpass filter," *IEEE Microwave and Wireless Components Letters*, vol. 18, pp. 590-592, 2008.

[28]   A. Tombak, F. T. Ayguavives, J. Maria, G. T. Stauf, A. I. Kingon and A. Mortazawi, "Low voltage tunable barium strontium titanate thin film capacitors for RF and microwave applications," *IEEE MTT S Int. Microwave Symp. Dig*., vol. 3, pp. 1345-1348, 2000.

[29]   L. Dussopt, "Intermodulation distortion and power handling in RF MEMS switches, varactors, and tunable filters," *Microwave Theory and Techniques, IEEE Transactions on*, G. M. Rebeiz, Ed. 2003, pp. 1247-1256.

[30]   C. L. Goldsmith, Z. Yao, S. Eshelman and D. Denniston, "Performance of low-loss RF MEMS capacitive switches," *IEEE Microwave Guided Wave Lett*., vol. 8, pp. 269-271, 1998.

[31]   E. Fourn, A. Pothier, C. Champeaux, P. Tristant, A. Catherinot, P. Blondy, G. Tanne, E. Rius, C. Person and F. Huret, "MEMS switchable interdigital coplanar filter," *Microwave Theory and Techniques, IEEE Transactions on*, vol. 51, pp. 320-324, 2003.

[32]   M. J. Howes and D. V. Morgan, "Variable Impedance Devices," *Eds. New York*: Wiley, ch. 1.

[33]   I. Hunter and J. D. Rhodes, "Electronically Tunable Microwave Bandpass Filters," *Microwave Theory and Techniques, IEEE Transactions on*, vol. 30, no. 9, pp. 1354–1360, 1982.

[34]   Shu, Y.H., Navarro, J.A., and Chang, K.: 'Electronically switchable and tunable coplanar waveguide-slotline band-pass filters', *IEEE Trans. Microw. Theory Tech*., 1991, 39, pp. 548–554

[35]   Liang, X.P., and Zhu, Y.F.: "Hybrid resonator microstrip line electrically tunable filter". *IEEE MTT-S Int. Microw. Symp. Dig.,* 2001, pp. 1457–1460

[36]   R. Zhang, and R. R. Mansour, "Novel digital and analogue tunable lowpass filters", *Microwaves, Antennas & Propagation*, IET, pp. 549-555, June 2007.

[37]   V. Miraftab, M. Yu, "Generalized Lossy Microwave Filter Coupling Matrix Synthesis and Design Using Mixed Technologies", *Microwave Theory and Techniques, IEEE Transactions on*, vol. 56, pp. 3016-3027, 2008.

[38]   V. Miraftab, M. Yu, "Advanced Coupling Matrix and Admittance Function Synthesis Techniques for Dissipative Microwave Filters", *Microwave Theory and Techniques, IEEE Transactions on*, vol. 57, pp. 2429-2438, 2009.